Cleaving to Connect:

Non-Free Radical Photopolymerization for Orthogonal Multi Material Volumetric Bioprinting of Hydrogels

Master Thesis Major Research Project

Michaël Hanna

E-mail: (m.hanna@students.uu.nl; m.a.hanna@pm.me)
Student number: 3288544
Master Program: Drug Innovation, Utrecht University
Examiner: Associate Professor Dr. Ir. R. Levato, Department of Orthopeadics, University Medical Center Utrecht, Departments of Clinical Sciences, Equine Sciences, Equine Musculoskeletal Biology, Faculty of Veterinary Medicine, Utrecht University (r.levato@uu.nl)
Second Examiner: Prof Dr. Ir. T. Vermonden, Department of Pharmaceutics, Faculty of Beta Sciences, Utrecht University (t.vermonden@uu.nl)
Daily Supervisor: Marc Falandt, MSc, Department of Orthopeadics, University Medical Center Utrecht, Departments of Clinical Sciences, Equine Sciences, Equine Musculoskeletal Biology, Faculty of Veterinary Medicine, Utrecht University (m.falandt@uu.nl)

March 7, 2023

Foreword

Alongside the physical materials that were synthesized, this thesis is the abstract product of the intellectual journey of my major research project that has been an interesting and enjoyable experience for me. I would like to thank the coordinator of the master program Drug Innovation, Associate Professor Slijper for advising me on a suitable research project, that would fit my interests and competencies. It was her suggestion to contact Professor Vermonden, who brought Marc and me into contact.

I would like to thank my examiners Associate Professor Levato and Professor Vermonden for hosting me at their respective departments and for sometimes giving me practical guidance. A special thanks I owe to my supervisor, Marc Falandt who showed a great deal of enthusiasm and sometimes patience when explaining new concepts to me or when answering questions. His profound and detailed understanding of concepts stimulated my curiosity.

During the work in the lab, I received help from many people. I would like to thank the technicians, who introduced the laboratories and equipment to me. Mies van Steenbergen has been a great help, not only in advice but also for making inquiries to other technicians from the NMR department for us. My gratitude also extends to the other technicians who have helped me, Mattie van Reijen, Anneloes Mensinga, Elianne Angela, Kim van der Wurff, Esmeralda Bosman, and Roel Maas-Bakker.

The PhD students have been very helpful and have helped me with parts of the experiments during this internship: Erik Hebels, Greta Di Marco, Matej Dzurov, Dmitrii Ludin, Eleonora Hochreiner, and Martina Viola for their help and advice in the synthesis lab. I also would like to thank Sammy Florczak for help with some light irradiation set-ups and an attempt to use his custom volumetric printer.

There are also many people who have not been involved with my work, but who were around the labs and office areas and contributed to the enjoyable atmosphere at both departments, my fellow students, and researchers in other research groups.

My thanks to all.

Michaël Hanna

Layman summary

The Biofabrication field seeks ways of producing organs by Bioprinting which is the 3D printing of cells and other tissue components. The materials used for this 3D printing are network forming molecules that can trap water, forming hydrogels. Examples of these are gelatin, hyaluronic acid, or the synthetic polymer polyethylene glycol (PEG). Networks are formed by bonding interactions named cross-links of chemicals groups having binding interactions. Blends of these hydrogels with cells and other tissue molecules are called bio-inks. Hydrogels are important in Bioprinting as they offer structural integrity and provide cells with aqueous environments. Traditionally, the more aqueous, the easier cellular interactions and tissue culture medium uptake, which are fundamental for tissue growth.

Older Bioprinting techniques involve contact Bioprinting, meaning that bio-inks are in physical contact with the printers. This is not beneficial for cells, especially in techniques where bio-inks pass through a nozzle where they are compressed and stressed. Contact Bioprinting is done by printing multiple layers on top of one another. Limitations are needs for supports in case of overhang structures and slow printing speeds. The latter is suboptimal for cells since they are separated from nutrient containing culture medium during printing.

Contactless Bioprinting generally is better for cells, as it does not stress cells physically and usually much faster. Volumetric Bioprinting (VBP) uses stimuli responsive bio-inks, commonly gelatin based, that respond to light. These bio-inks contain an additional photo-initiator to start the cross-linking of the hydrogel. These photo-initiators are cleaved by light irradiation to produce free radicals. The hydrogels have reactive groups that cross-link because of these free radicals, forming solid constructs. VBP works by light irradiation through bio-inks in 2D fashion, using tomographic projections which can be compared to a CT scan. Rotating the platform results in 360-degree irradiation and printing of 3D constructs. Though showing promise, free radicals are uncontrollable and perform side reactions with adverse effects, such as cell damage. In case of printing with different hydrogels, selective cross-linking is not possible because they react with multiple hydrogels simultaneously. As native tissues comprise different materials, multi material printing methods are essential.

This thesis demonstrates cross-linking without free radicals by use of maleimides and thiols, that cross-link spontaneously. Two hydrogels with respectively either thiols or maleimides were used. For controlled cross-linking, a green light absorbing photocleavable protecting group (PPG) was placed onto the thiols of a PEG hydrogel. A PPG is a molecule that is attached to a reactive group, making it unavailable to fulfill its original function. Depending on their molecular structure, PPGs can absorb specific light wavelengths. Only when they are irradiated with wavelengths that they absorb, they are released, thus making the reactive groups available. This hydrogel was incubated with a maleimide containing hyaluronic acid hydrogel and due to the PPG, selective green light-controlled cross-linking was achieved using VBP.

Future VBP developments lie in using multiple different PPGs combinations with different hydrogels that use different spontaneous cross-linking mechanisms. A requirement is that the PPGs do not have overlapping absorbance and that the cross-linking mechanisms are selective.

Abstract

The Biofabrication technique of Bioprinting is used for the goal of printing native tissues. While older contact Bioprinting techniques are not sufficient for this goal, the recent technique of volumetric bioprinting (VBP) has significant advantages, such as high printing speeds and absence of physical contact with bio-inks, benefitting cellular conditions. Currently, main VBP limitations are lack of material variety and use of free radical cross-linking. Printing of native tissues requires both limitations to be resolved. Material variety since native tissues are comprised of multiple materials and free radicals due to their high reactivity, which is incompatible with bioorthogonal printing. In this thesis, spontaneous cross-linking thiol-maleimide chemistry was used in combination with a green light absorbing coumarin based photocleavable protecting group (PPG). Hyaluronic acid was functionalized with maleimide (HA-MAL) and two PEG thiol linkers, one single PEG and one larger PEG of 5 kDa molecular weight (MW) were protected by the PPG. Since the used PPG has low water solubility, the longer PEG chain was used to improve water solubility to create the hydrogel networks. Addition of organic solvents to further improve solubility proved to be ineffective, due to reduction of thiol-maleimide cross-linking kinetics. HA-MAL and PEG form a hydrogel at low concentrations of respective 0.6% and 0.3% w/w concentrations, which is optimal for cells. Printing at λ_{max} of 473 nm yielded gelation, but for printing purposes absorbance will be too high. Use of lower absorbance at 520 nm proved to be possible as well and is preferable due to increased transmission and decreased scattering. Maleimide degradation is important to prevent before printing but is not an issue after printing. Maleimide degradation can be minimized by keeping it in acidic conditions and only adjusting it to physiological pH just before printing, which is needed for cross-linking. This does require an effective buffer while being isotonic to cells. The main refinement that should be considered is increasing water solubility to improve printability and the ability to filtrate materials, as sterile materials are required when printing with cells. Future bioorthogonal VBP may be achieved by use of multiple PPGs and combinations of multiple spontaneous cross-linking mechanisms.

Table of Contents

List of Abbreviations

4arm PEG	4arm Polyethylene Glycol 5000 (Thiol)4
4-DMAP	4-Dimethylaminopyridine
4-NPC	4-Nitrophenylchloroformate
ACPC	Articular Chondroprogenitor Cell
ACN	Acetonitrile
DCC	N,N'-Dicyclohexylcarbodiimide
DCM	Dichloromethane
DoF	Degree of Functionalization
DMF	Dimethylformamide
DMF-DMA	N,N-Dimethylformamide dimethyl acetal
DMD	Digital Mirroring Device
DLP	Digital Light Processing
EBB	Extrusion Based Bioprinting
EDC	N-ethyl-N'-(3-(dimethylamino)propyl)carbodiimide hydrochloride
EDT	2,2'-(Ethylenedioxy)diethanethiol
EU	European Union
ECM	Extracellular Matrix
GelMA	Gelatin-Methacryloyl
GPC	Gel Permeation Chromatography
HA	Hyaluronic Acid
HA-MA	Hyaluronic Acid Methacrylate
HA-MAL	Hyaluronic Acid Maleimide
HCl	Hydrochloric Acid
Linear PEG	Polyethylene Glycol 2000 or 5000 (Maleimide)2
LbL	Layer-by-Layer
LAP	Lithium Phenyl-2,4,6-Trimethylbenzoylphosphinate
LiCl	Lithium Chloride
LIFT	Laser-induced Forward Transfer
MAA	Methacrylic Anhydride
MES	Morpholinoethanesulfonic Acid Sodium Salt
$MgSO_4$	Magnesium Sulfate
MSC	Mesenchymal Stem Cell
MW	Molecular Weight
$NaHCO_3$	Sodium Hydrogen Carbonate
$NaIO_4$	Sodium(meta)persulfate
NHS	N-Hydroxysuccinimide
NMR	Nuclear Magnetic Resonance
PBS	Phosphate Buffered Sodium solution
PI	Photo-Initiator
PPG	Photocleavable Protecting Group
PQ	9,10-Phenanthrenequinone
RC	Regenerated Cellulose
RM	Regenerative Medicine
ROS	Reactive Oxygen Species
SLA	Stereolithography
TE	Tissue Engineering
THF	Tetrahydrofuran
UCST	Upper Critical Solution Temperature
VBP	Volumetric Bioprinting
VE	Vinyl Ether
ViV	Volume-in-Volume

1   Introduction

1.1   A breakthrough in organ replacement strategies is needed

In 2019, 34285 transplantations were conducted within the European Union (EU), while the number of patients needing a transplantation was threefold higher.[1] This imbalance is caused by a shortage of organs available to patients, resulting in waiting lists of three to five years, depending on the needed type of transplant.[2] While waiting, quality of life will be lowered and 3.2-3.9% of patients die unnecessarily.[1] Governments have tried to increase the number of donors by various methods, such as increasing citizens' awareness and streamlining internal processes within healthcare ministries.[3] Unfortunately, such methods have led to a marginal increase only. The average yearly rise in transplantations in the EU between 2010 and 2019 was 522, with a substantial decline in the latter two years.[1] Therefore, a breakthrough in organ replacement strategies is needed, which lies in advancing biotechnological solutions.

1.2   Biofabrication and Bioprinting

1.2.1   Biofabrication to recreate tissues

Biofabrication is used today to study how combinations of cells, biomaterials, and signals such as growth hormones can be used in constructing new tissues with the aim to recreate native functional tissues.[4] Schematized in Figure 1, Biofabrication is based on combining the fields of Tissue Engineering (TE) and Regenerative Medicine (RM), although the term is used in other disciplines as well. Whereas conventional TE and RM techniques focus on the growing of tissues, Biofabrication has a specialized focus on improving spatial control, indirect via Bioassembly or direct via Bioprinting, the subject in this thesis.[5]
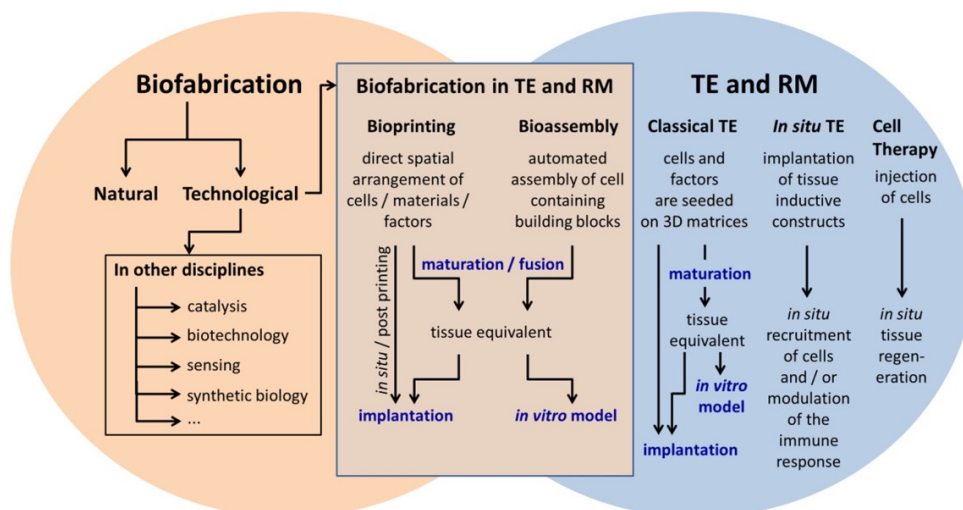
Figure 1: The field of Biofabrication within TE and RM.[5] Left: The term Biofabrication is used for a variety of concepts across different disciplines. Middle: Biofabrication within TE and RM comprises Bioprinting and Bioassembly. Right: Conventional TE and RM techniques are focused on the growing or regeneration of tissues.

1.2.2   Bioprinting

Bioprinting is the bio-engineering of functional (micro)tissues by means of computer aided patterning and assembling of cells and non-living materials in a specific 2D or 3D organization.[6] Contact – and contactless Bioprinting can be distinguished, the former meaning that the printed materials come in physical contact with the printer which is not the case in the latter.

1.2.2.1 Contact Bioprinting

Contact Bioprinting comprises mostly more classical 3D Bioprinting techniques, which came in the wake of revolutionary improvements in the field of additive manufacturing. Additive manufacturing is the layer-by-layer (LbL) deposition of material to create a 3D structure. A software algorithm is usually used to convert a 3D image of the desired construct into 2D splices in a vertical manner. The 2D layers are then printed one-by-one, stack wise. These stacked layers should then represent the 3D image. In Bioprinting, used materials are biocompatible, and may contain cells. The latter are often processed in hydrogels, referred to as bio-inks.[7] Hydrogels' aqueous 3D environment is suitable for simulating the extracellular matrix (ECM).[7] In Biofabrication, such hydrogels are based on naturally derived polymers, such as hyaluronic acid, gelatin, alginate, and collagen.[7]

Additive manufacturing

Additive manufacturing techniques that are applied in Bioprinting are laser-induced forward transfer (LIFT), inkjet printing, and the extrusion-based technique robotic dispensing, shown in Figure 2. With LIFT *(A)*, the bio-ink is covered by an energy absorbing layer.[8] When a laser hits the energy absorbing layer at a specific place, evaporation occurs.[8] This results in a gas pressure, propelling a droplet of bio-ink to the collecting plate.[8] In inkjet printing *(B)*, the bio-ink can be deposited using either a heater or a piezoelectric actuator within a nozzle, resulting in a small droplet of bio-ink.[9,10] LIFT and inkjet printing are small scale. Dispensing larger hydrogel strands is done by robotic dispensing *(C)*, a common Extrusion Based Bioprinting (EBB) technique. Although faster than the previously mentioned techniques, the resolution is lower.[11] Due to wide material availability and affordability, EBB techniques are most widely in use currently.[12]
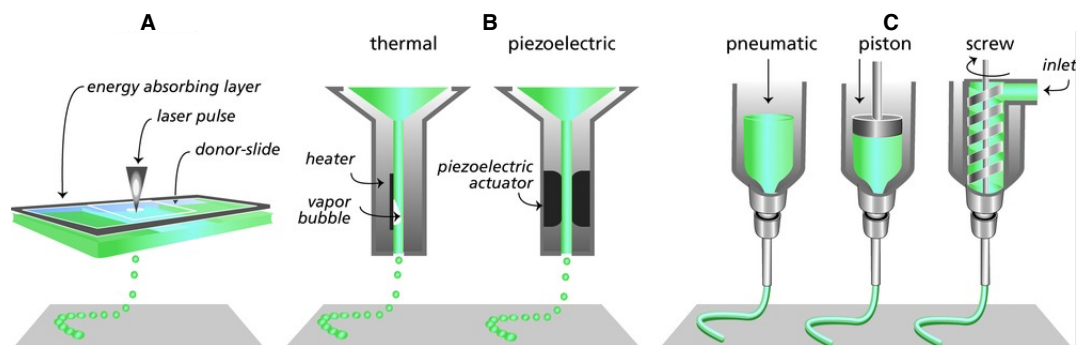

Figure 2: Classical 3D Bioprinting techniques. A: LIFT. B: Inkjet printing. C: robotic dispensing.[7]

Bioinks

Bio-inks are mostly soft materials, as they commonly consist of hydrogels which may contain cells, extracellular matrix molecules, and cell signaling molecules. They contain high water percentages, as cells need aqueous environments. This creates a difficulty in maintaining the shape-fidelity of the individual layers printed by LbL bioprinting techniques, as the layers need to be capable of supporting not only their own weight, but the total weight of the subsequently stacked layers.[13] One method of improving shape fidelity is using scaffolds. These are harder biocompatible and biodegradable polymers with a high shape fidelity onto which bio-inks are dispensed. The idea is that after a construct is produced, the cells in the bio-ink mature, following the shape of the scaffold and thus grow into the designed tissue. Scaffolds are designed to degrade after an intended time – depending on tissue type – in which they are replaced by the growing number of cells.

Besides scaffolds, shape fidelity can be improved by choice of hydrogel, to have increased surface tension or other mechanical or physical forces. Also, printed constructs need to have a certain degree of stiffness, a measure of how well the construct keeps its length.[14] Stiffness can be increased by means of cross-linking of the polymer molecules within the hydrogel, either partially before or directly after printing.[15] Cross-linking of polymers, demonstrated in Figure 3, is the binding that occurs between chemical groups on the polymer molecule that become reactive under certain stimuli, such as γ-radiation,[16] X-rays,[17] hν light,[18] heat,[19] sound,[20] addition of cross-linking agents,[21] and others. Although usually covalent, non-covalent cross-linking is also possible by using supramolecular[22] or dynamic covalent bonds.[23] Because of the newly formed networks, the polymer molecules, potential cells, and water are held in place. Both physical entrapment of cells and the subsequent osmotic forces are responsible for this.
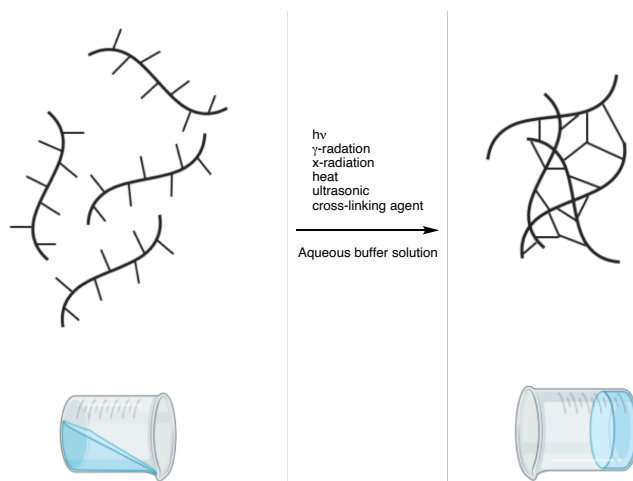
Figure 3: Hydrogel formation after cross-linking by a variety of stimuli possibilities.

Stereolithography

The principle of stereolithography (SLA) is use of light as a stimulus for cross-linking.[24] In the more recent SLA technique Digital Light Processing (DLP), a digital micromirror device (DMD) is used to irradiate a layer of a bio-ink with light. Shown in Figure 4, light is projected onto a motorized stage which is submerged in a bio-ink.[25] After polymerization of an entire layer at once, the stage in contact with the construct lowers, and another layer is constructed above the previous one.[25] Repeating this process for each layer results in the 3D construct.[25] For each layer and depending on the desired shape of the construct, the DMD alters the irradiation pattern.[25]

Figure 4: Schematic of a DLP set-up.[25]

1.2.2.2 Limitations of contact Bioprinting

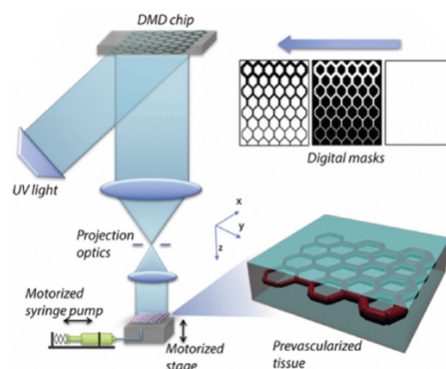General bio-ink limitations have been schematized in the biofabrication window, shown in Figure 5.[7] For printability in case of covalent cross-linking and depending on the material, higher cross-link density results in stiffer gels that are higher in shape fidelity.[26] However, aqueous environments are more optimal for cells, as their migration, proliferation, and differentiation are not limited by dense polymer networks.[7] The compromise between these factors is known as the biofabrication window.[7]
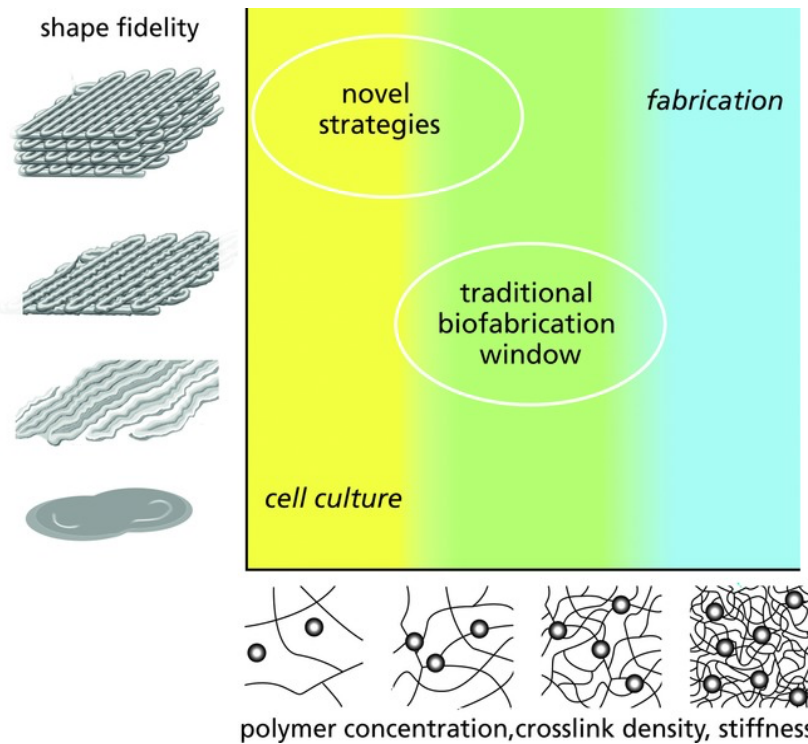

Figure 5: The traditional biofabrication window.[7] The right side in blue represents optimal fabrication conditions with stiff materials, higher polymer concentrations and cross-link densities. The left side in yellow represents optimal cell culture conditions, with opposite properties.

A particular limiting factor in extrusion and inkjet Bioprinting is the nozzle through which bio-inks are extruded. During printing, compressive and rheological forces are applied on the bio-ink, affecting printability – a measure of how well the printing process occurs –, shape fidelity, and cell behavior.[15] Different cell types may respond differently to deformation, leading to the activation or inhibition of signaling cascades that influence their behavior undesirably.[27] Printing of larger cell aggregates or fragile organoids is not optimal. Although LIFT is nozzle-free, the technique is low in printing efficiency, repeated coating is needed for each layer of ink, and uniformity is not guaranteed.[28]

A particular limiting factor in DLP are the optical requirements of the bio-ink. Polymerization of one layer at a time means that all the light should be absorbed by that specific layer. If this is not the case, the earlier polymerization layers will receive an additional light dose and over polymerization will occur. This has been solved by adding photo absorbers,[29] although generally, few biocompatible materials that fulfil the optical requirements for DLP exist.

A common downside of all techniques mentioned so far is their slow printing speed. During printing, bio-inks sustain sub optimal cellular conditions. Cells are removed from culture

medium and undergo temperature changes. Slow printing speeds are also sub optimal for all printing processes, as bio-inks with cells are suspensions. In case of very long printing times, this means that they can be subject to sedimentation, particle size distribution changes, and other effects that apply to suspensions. Such effects will worsen uniformity, as the bio-inks at the end of printing are different compared to the start. Thus, slow printing speed limits printing of larger, more complex functional tissues.

A final drawback of contact bioprinting is the requirement for supportive materials in case of overhanging designs. Illustrated in Figure 6, the printing of overhangs with soft materials results in low shape fidelity (*A*), unless supportive materials are used (*B*). This severely limits the freedom of design, as complex designs require many supports. Besides the illustrated example in extrusion printing, this limitation applies to all contact bioprinting techniques. Freedom of design was increased by embedded printing,[30] meaning that printing is not done in air, but in a supportive bath. As support baths may interact with the printed bio-inks and with the printers, they need to fulfill various criteria, adding complexity. A key difficulty of embedded printing lies in separating the support bath from the printed constructs without affecting them.[31]
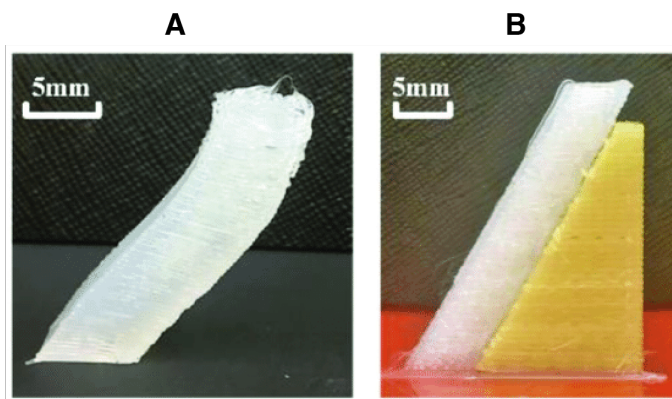

Figure 6: Illustration of required support materials in extrusion printing. Adapted from Muthusamy et al.[32] A: Printed silicone without supports. B: Printed silicone with supports, shown in yellow.

1.2.2.3 Contactless Bioprinting
Contactless Bioprinting yields 3D constructs without printer components physically interacting with bio-inks. As a result, many of the limitations mentioned previously are absent. A major advantage is absence of physical stresses on cells. Also, when considering the biofabrication window (Figure 5), a shift in usable bio-inks towards cell culture medium is possible due to reduced rigidity requirements for fabrication. Contactless Bioprinting has been achieved by patterning of cells by magnetism,[33] sound,[34] and light.[28]

1.3   Volumetric Bioprinting
Volumetric Bioprinting (VBP) is a powerful light based contactless Bioprinting innovation, due to its very high printing speed compared to all other techniques in use thus far.

1.3.1   Mechanism
VPB works by having a vat containing a light sensitive bio-ink connected to a turning motor, which can be irradiated by 2D tomographic projections through a digital light processing (DLP) modulator.[35] When the motor turns the vat, multiple 2D light patterns are being irradiated in

a 360-degree fashion, illustrated in Figure 7 *(A)*. The shape and sequence of the 2D light patterns are controlled by a computer algorithm that uses Radon transform to calculate the correct light intensity, so that the cumulative effect of the 2D projections is analogous to a 3D projection *(B, C)*.[35,36] Since constructs are printed within a volume, VBP can be called a volume-in-volume (ViV) technique.
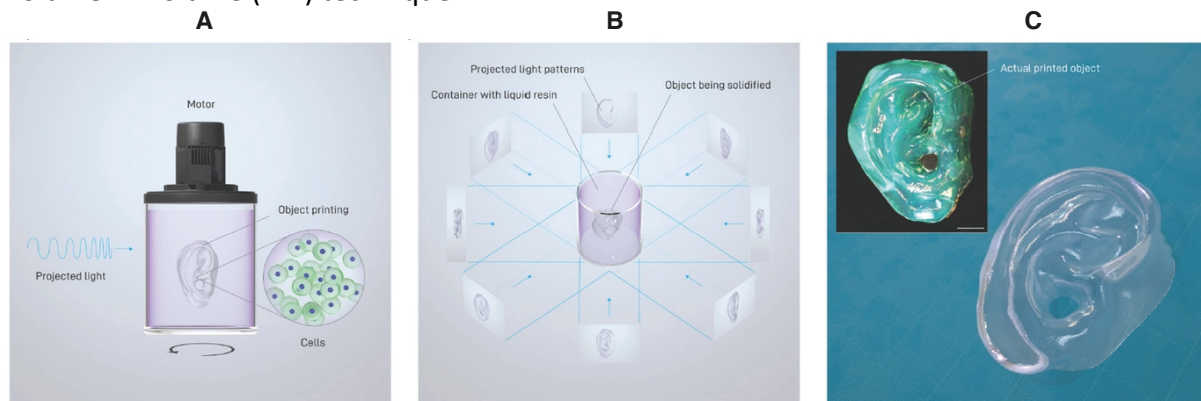

Figure 7: Schematic overview VBP.[35] A: A motor turns the vat containing a bio-ink, with a single light source. B: A software controlled DLP modulator projects light in 2D, whilst accounting for the turning of the vat to create a 3D print. C: Printed construct.

1.3.2 Achievements thus far

High shape fidelity printed constructs have been printed at impressive speeds. Bernal *et al.* showed the printing of menisci-like and trabecular bone-like tissues, using respectively articular chondroprogenitor cell laden (ACPC) and equine mesenchymal stem cell (MSC) laden gelatin-based bio-inks within tens of seconds using a laser source at 405 nm.[35] In a follow-up study, Bernal *et al.* demonstrated printing with human liver epithelial organoids in a similar gelatin based bio-ink into liver-like tissue using the same printer within 20 seconds.[37] Bone-like tissue was printed within 30 seconds using a similar printer set-up by Gehlen *et al.* with a gelatin-based bio-ink containing human MSCs.[38] Rizzo *et al.* printed skin constructs containing normal human dermal fibroblasts (NHDFs) in 10 seconds, also using a similar printer set-up combined with a gelatin based bio-ink.[39]

1.3.3 Material properties

The use of gelatin-based hydrogels in all studies mentioned above is not a coincidence. Due to the requirement of biocompatibility, commonly used monomers, macromers, or oligomers that are responsible for the hydrogel properties are derived from natural sources.[40] Their added value over synthetic polymers is intrinsic possession of biological epitopes and signaling capabilities.[41] At the same time, materials should be sensitive to light to form cross-links and to solidify. Opposite to DLP, VBP resins should be transparent as the printing process is ViV rather than LbL.

1.3.3.1 Gelatin

Gelatin has thermal gelation properties, where it is soluble in water above the upper critical solution temperature (UCST) of 30 °C.[42] Below the UCST it is a gel. Gelatin use in VBP capitalizes on the many functional side groups, such as amino, hydroxyl, and carboxylic groups,[43] allowing for chemical modifications to cross-link via alternative mechanisms. The most common modification is the generation of methacrylates and methacrylamides by conjugation of methacrylic anhydride (MAA) to gelatin's hydroxyl and amino groups, shown in Scheme 1 *(A)*. The percentage of hydroxyl and amino groups that are conjugated is referred

to as the Degree of Functionalization (DoF).[44] Since a combination of functional groups is usually achieved, the gelatin is known as gelatin methacryloyl (GelMA). These new functional groups form cross-links under hν light and in the presence of a photo-initiator (PI), such as lithium phenyl-2,4,6-trimethylbenzoylphosphinate, used in all referenced VBP articles. PIs are cleaved upon light irradiation within their absorbance spectra, and free radicals are generated *(B).* Subsequent free radical mediated polymerization occurs *(C)*, yielding solid constructs *(D).*

A GelMA synthesis

B LAP cleavage to produce radicals

C Radical mediated cross-linking

Continuation or termination

D GelMA in solution before and after cross-linking

hν, LAP

PBS
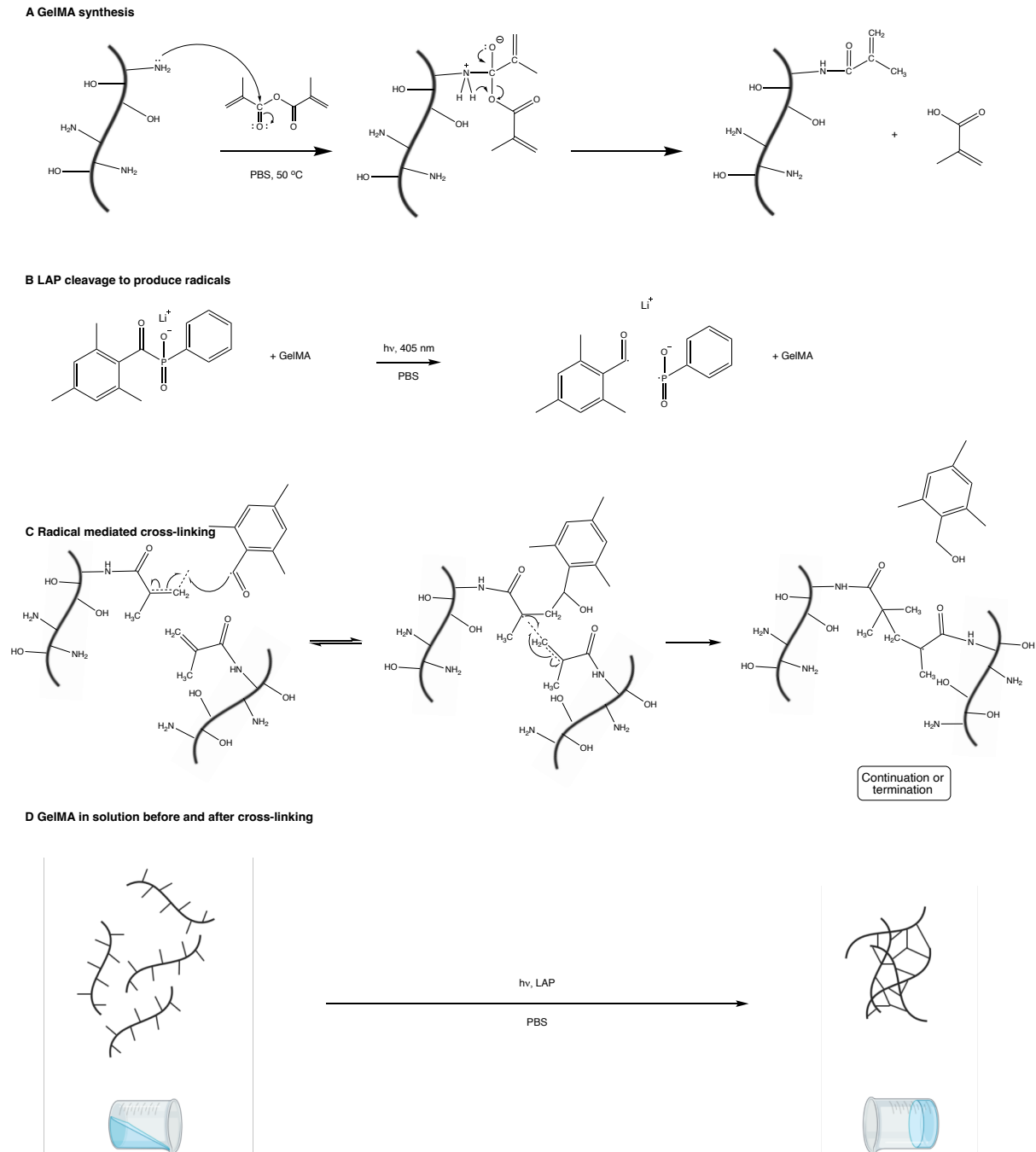
Scheme 1: A: Conjugation of MAA to gelatin. A nucleophilic addition of the amine to the carbonyl may occur. As a result of the newly formed bond, one electron-pair of the double bond adds to the oxygen atom, giving it a negative charge. This extra electron pair is favored to form the C=O double bond. The electrons of the ester bond add to the oxygen, after which protonation occurs and the ester is cleaved. B: LAP PI photocleavage results in radical formation. C: Potential mechanism of radical mediated cross-linking of two or more MAAs. D: Before cross-linking, GelMA occurs in solution. After cross-linking, it forms a hydrogel.

1.3.3.2 Hyaluronic Acid

Another ECM derived oligomer that is commonly used in hydrogels is hyaluronic acid (HA).[45] It contains the disaccharide units D-glucuronic acid and N-acetyl-D-glucosamine in a repetitively, and is a nonsulfated glycosaminoglycan.[40] Since it has a role in cell differentiation, - migration, and - growth, it is highly biocompatible.[46] Like gelatin, HA also possesses many functional groups: primary and secondary hydroxyl and carboxylic acid groups. Hyaluronic acid methacrylate (HA-MA) is commonly synthesized by conjugation of MAA to primary hydroxyl groups in aqueous environment (Scheme 2).[47,48] The reaction and polymerization mechanisms are similar to GelMA.
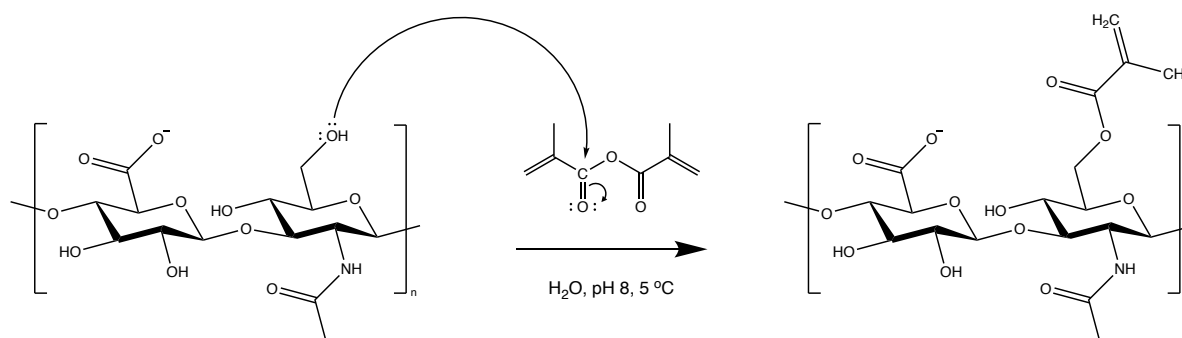
Scheme 2: HA-MA synthesis by conjugation of MAA to HA.

More combinations of other oligomers and functionalization types are possible, and these affect the properties of the final construct. Furthermore, there are several methods to tune a bio-ink and the process of VBP, listed in Table 1. Generally, a hydrogel can be made stiffer by increasing the concentration of the oligomer that forms the hydrogel.[44] Also, the DoF influences the number off cross-links that can be made, correlating to hydrogel stiffness.[44] Additives can be added to hydrogels that change the rheological behavior. Examples are gellan gum and nanoparticles.[49,50] Apart from stiffness, also the construct pore size and cell spreading can be influenced by these parameters.[44]

Table 1: Tunable properties of GelMA in bioprinting.[44]

Tunable parameters	Final construct properties
Hydrogel concentration	Cell spreading
Degree of functionalization	Pore size
UV intensity	Hydrogel stiffness
Rheological additives	

1.3.4   Limitations

The strength of VBP is also a challenge: the completion of a whole construct within one step means that it will be difficult to print using multiple bio-inks in a controlled manner. As a result, the printing of multiple layers of different cell types is more difficult to reliably achieve compared to classical 3D Bioprinting methods. Thus far, only one very recent publication demonstrated multi-material VBP.[51]

1.3.4.1 Sequential printing

One reason for this lies in the physicochemical properties of the bio-inks used in VBP in relation to the printing procedure: Constructs are printed below the UCST. After printing, temperature is raised to above the UCST to wash away non-cross-linked bio-ink, usually

around 37 °C with phosphate buffered sodium solution (PBS). To print a second 3D layer, the second bio-ink should be added, and the temperature should be brought then hypothetically below the UCST. It is important to secure the construct in a fixed place, to have the starting position of the rotation in relation to the light source the same as before. Otherwise, light will be irradiated in incorrect patterns, resulting in over- and undercuring of certain areas of the construct.

In addition, constructs printed by VBP can be subject to a degree of shrinkage or swelling,[52] after printing. An interplay of temperature and/or osmotic forces (when washing away the uncross-linked hydrogel with PBS) and the construct itself occurs. The way in which this happens may depend on the bio-ink that is used: different hydrogels and different cell types will have different physicochemical properties. Taking this appropriately into account forms another difficulty in printing multi-components by VBP.

1.3.4.2 Free radicals
Although it can be controlled for when free radicals are formed, it cannot be controlled how they react afterwards due to their high reactivity. As a result, they are not only involved in cross-linking, but also in uncontrolled side reactions. Thus, they are incompatible with bioorthogonal printing. An example of such a side reaction involves cytotoxicity when they form reactive oxygen species (ROS) when encountering molecular oxygen. ROS have been known to be involved in cell death and damage in many ways, such as apoptosis,[53,54] necrosis,[54] damage to cell transporters,[55] and DNA and RNA damage.[56–58] The extent of these on the bioprinting process partially depends on factors such as PI concentration and the cell type used. For example, when using a bio-ink with differentiating stem cells, eliminating potential cell damage is essential.

More importantly, in case of moving towards printing of native tissues by using multiple bio-inks, free radicals will react non-orthogonally. In case of one material printing such as using only GelMA or HA-MA, this is not an issue. However, in case of multi material printing, for example by combining GelMA and HA-MA, free radicals may react with both materials uncontrollably. Even changing the reactive groups of one bio-ink will not be enough, as free radicals are highly reactive and can react with many groups in various reaction types.[59]

1.4   Photocleavable Protecting Groups
1.4.1   Mechanism
Photocleavable Protecting Groups (PPGs) have been used as means of making available functional groups at will by light in various applications.[60,61] Mechanisms by which this occurs are based mostly on hν light.[60,61] The principle is that these groups are conjugated to a molecule's functional group. This makes the functional group unavailable to other molecules that may react to it.[60,61] Only when light stimuli at specific wavelengths are applied, PPGs are cleaved, and the previously protected functional groups become available for a reaction with molecules from its environment.[60,61]

1.4.2   Advantages
Various types of compounds have been discovered to be useful to serve as PPGs that are bioorthogonal, such as salicyl alcohols,[62] nitrobenzyl -,[63] arylmethyl -,[64] and coumarin

compounds.[60,61] Moreover, they can be chemically modified to make them wavelength selective. In case of the protection of chemical groups that are spontaneously reactive, it means that free radical cross-linking mechanisms can be omitted. Within VBP, this is a potential method for true orthogonal printing.

1.4.3 Coumarin PPGs

Depending on the chemical structure, coumarin derivatives are low in cytotoxicity.[65] In case of coumarin PPGs, several modifications have been done to alter their photodegradable properties by a light range from near ultraviolet (300 nm) to green light (500 nm), shown in Figure 8.[61]
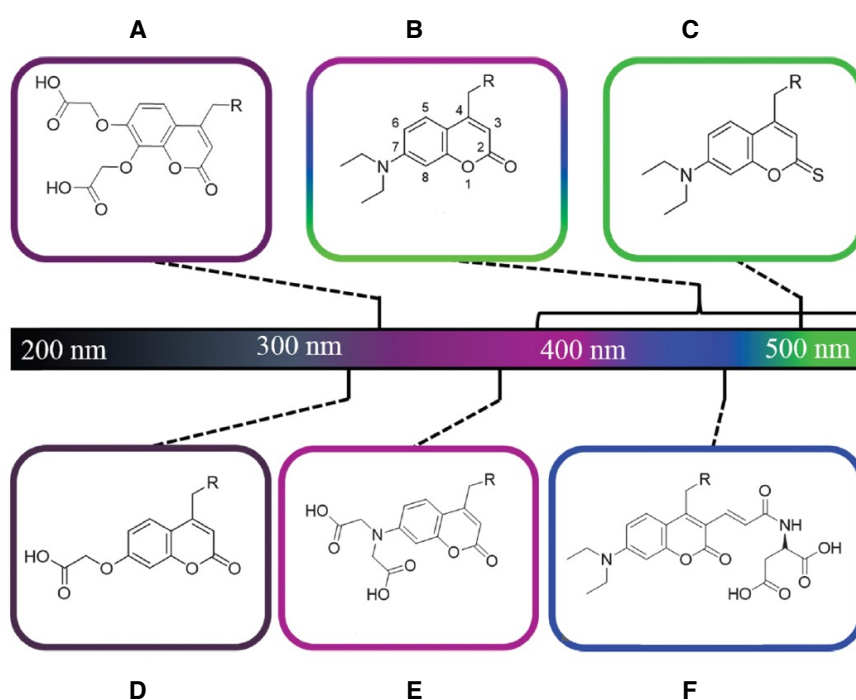

Figure 8: Overview of coumarin modifications on wavelength photocleavage potential, adapted from Hansen et al.[61] A: Carboxymethoxy substitutions showed an Abs_{max} at 324 nm.[66] B: Addition of a diethylamino group increases the Abs_{max} to ±400 nm,[67,68] although slow photocleavage at higher wavelengths has been observed.[69] C: Thio-substitution of the carbonyl at the 2 position increases Abs_{max} to 500 nm.[65] D: Alkoxy group at the 7 position lowers Abs_{max} to 310 nm.[70] E: Dicarboxymethylamino group changes Abs_{max} to 360 nm.[71] F: The enoyl group changes the Abs_{max} to 450 nm.[72]

1.5 Hypothesis and aim

Moving towards multi material bioorthogonal VBP, this report revolves around the research question of how multi material VBP can achieved by using photocleavable protecting groups combined with different hydrogel materials.

1.5.1 Material selection

For this purpose, compound **C** of Figure 8 was selected as a PPG. The reason for this is that it is cleaved under green light. Since currently VBP is done using blue light, it means that printing can be achieved by novel use of another light wavelength. An added benefit is that compound **C** is synthesized from compound **B**, which works in blue light. Because both are part of the same synthesis pathway, an added benefit is that both compounds are available for use as PPGs. Hyaluronic acid was selected as another material for use in VBP as it is a well-established hydrogel compound that is naturally derived, like gelatin. This makes it a good choice for eventual printing with cells. Thiol-maleimide chemistry was used as a spontaneous

cross-linking mechanism. The advantage is that in polar solvents reaction speed is very high,[73] and catalysts and free radicals are not necessary.[74,75] The mechanism by which this occurs is first spontaneous thiolate dissociation from thiols,[76,77] shown in Scheme 3 (*A*). Next, an electrophilic addition under Markovnikov's rule can take place (*B*). The absence of free radicals makes it a good choice for improving bioorthogonality.
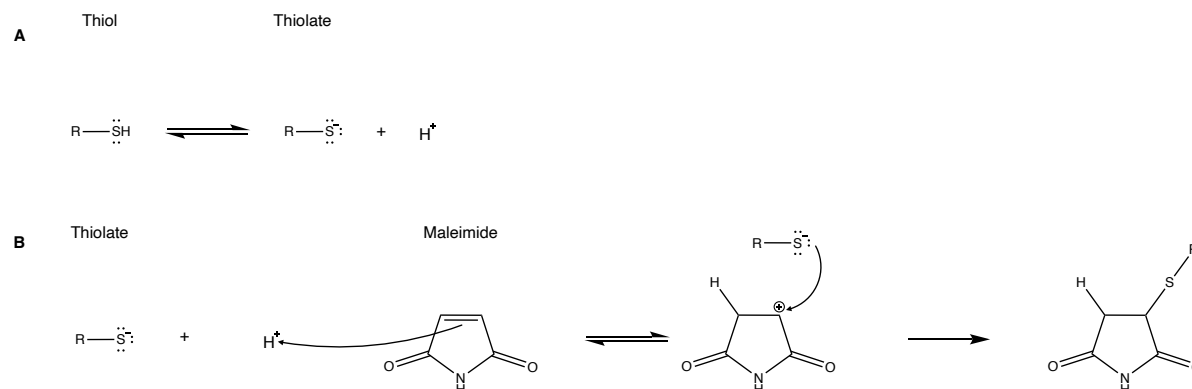
Scheme 3: Thiol-maleimide reaction mechanism in polar solvents. A: An equilibrium between thiol and thiolate occurs. B: Electrophilic addition of the thiolate to maleimide.

1.5.2 Approach

The mentioned selections were combined in the following approach: linear PEG maleimides (2 and 5 kDa MW) (referred to as *linear PEG*) were used with either a small linear PEG thiol (referred to as *EDT*) as cross-linker or a larger 4arm PEG thiol (5 kDa MW) (referred to as *4arm PEG*) which were both protected by a PPG for preliminary tests. Next, hyaluronic acid was functionalized with maleimide (referred to as *HA-MAL)* and used with *protected 4arm PEG*.

Subsequently they were used in VBP with green light, as seen in Figure 9. The thiols of a *4arm PEG* are protected by PPGs (*A*), rendering them unavailable to maleimides. Thus, no polymerization occurs. Upon light irradiation, the PPGs are cleaved, and thiols are available for conjugation (*B*). The thiols conjugate to maleimides, cross-linking the hydrogel molecules and solidifying the construct (*C*).

A successful proof of concept would open the doors for further developments on combining this approach with current VBP techniques and refinement of PPG use.
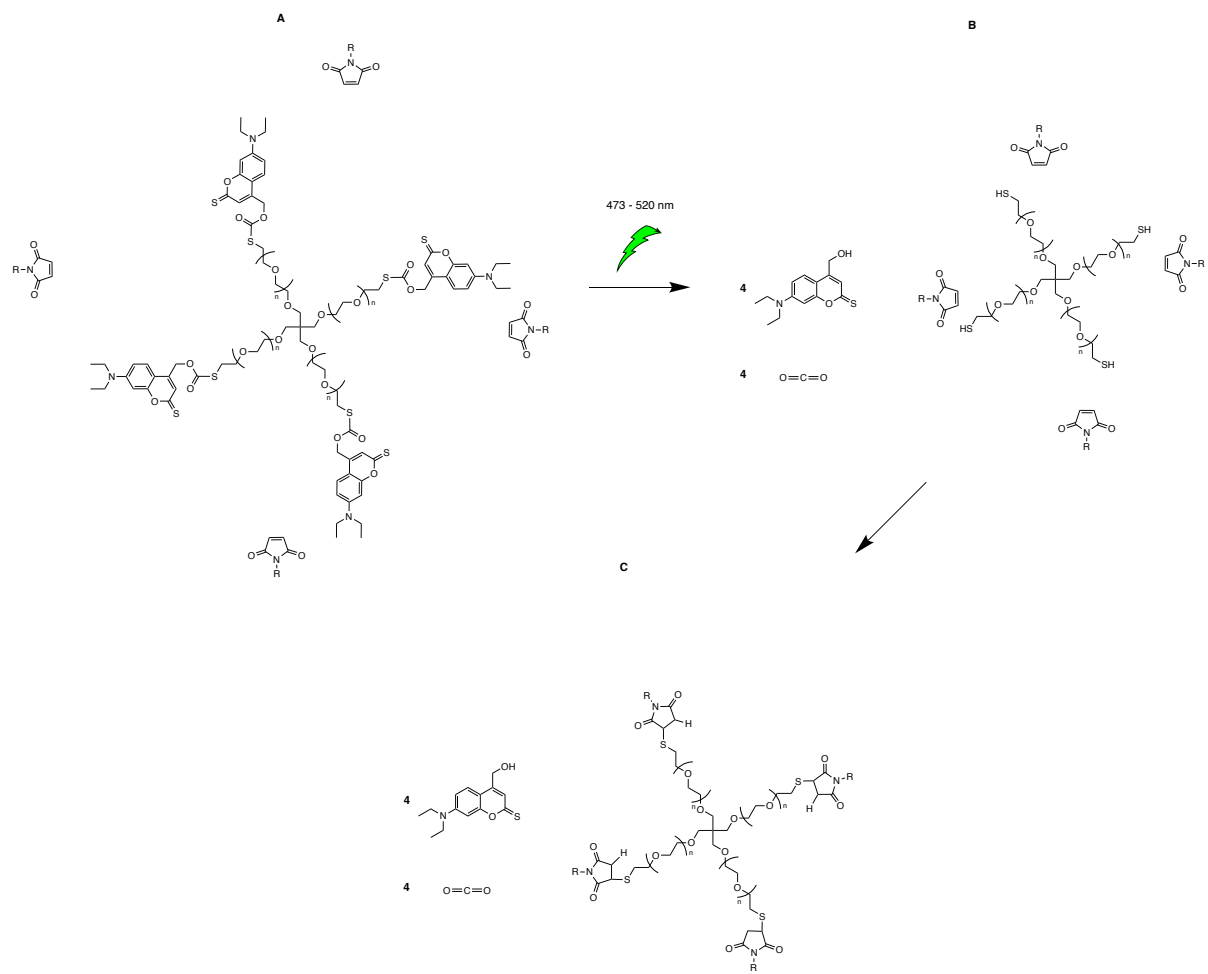
Figure 9: Light controlled cross-linking by a PPG and thiol-maleimide chemistry. A: Protection by PPGs of a four-arm PEG thiol. They are unavailable to the maleimides, conjugated to HA (-R group). B: Deprotection after green light irradiation. C: With available thiols, spontaneous cross-linking occurs.

2 Materials and Methods

2.1 Materials

RC sterile syringe filters (0.22 μm) were obtained from Corning Incorporated, USA. Whatman Gel Permeation Chromatography (GPC) filter vials (0.2 μm) were obtained from Cytiva, USA. CME sterile syringe filters (0.45 μm) were obtained from Carl Roth GmbH., Germany. Clear glass vials (1 mL, lot number i116-019) were obtained from Infochroma AG, Switzerland. Solution of Phosphate Buffered Saline (PBS), 10x concentrated, was obtained from Thermo Fisher Scientific, USA. Linear PEG (maleimide)2, 2 kDa and 5 kDa MW (lot numbers ZZ322P049 and ZZ328P163) and 4arm PEG (thiol)4, 5 kDa MW (lot number ZZ387P161) were obtained from JenKem Technology USA Inc., USA. Acetic acid, N,N'-Dicyclohexylcarbodiimide (DCC), 4-Dimethylaminopyridine (4-DMAP), and Hydrochloric acid (HCl) fuming 37% were obtained from Merck KGaA, Germany. Acetone, Dichloromethane (DCM), and Silica gel amorph 40-63 μm were obtained from VWR international S.A.S., France. 1-(2-Aminoethyl) maleimide hydrochloride and N-ethyl-N'-(3-(dimethylamino)propyl)carbodiimide hydrochloride (EDC) were obtained from Tokyo Chemical Industry Co., Ltd, Japan. Dimethylformamide (DMF), Ethanol absolute, Ethyl Acetate, Tetrahydrofuran (THF), and Toluene were obtained from Biosolve Chimie SARL, France. Sodium Hyaluronate from cockscomb (dried, containing 5% H_2O, 130 kDa MW, lot number 002941) was obtained from Lifecore Biomedical Inc., USA. Visking dialysis tubing with was obtained from SERVA Electrophoresis GmbH, Germany. Material properties were as follows: regenerated cellulose (RC), suitable for a pH range of 2-12, molecular weight cut-off (MWCO) of 12-14 kDa, pore diameter 25 Å. All other chemicals, unless stated otherwise, were obtained from Sigma-Aldrich, USA.

2.2 Methods

2.2.1 Synthesis

Protected EDT, *protected 4arm PEG*, and *HA-MAL* were synthesized (Figure 10). Structural confirmation of all components was done by nuclear magnetic resonance (NMR). Synthesis protocols and NMR spectra be found in the Supporting Information, Chapters S1 and S2. Unless stated otherwise, all NMR spectra were obtained using a 400-MR NMR spectrometer by Agilent Technologies, USA. All NMR spectra were analyzed using MestReNova version 14, by Mestrelab Research S.L., Spain.
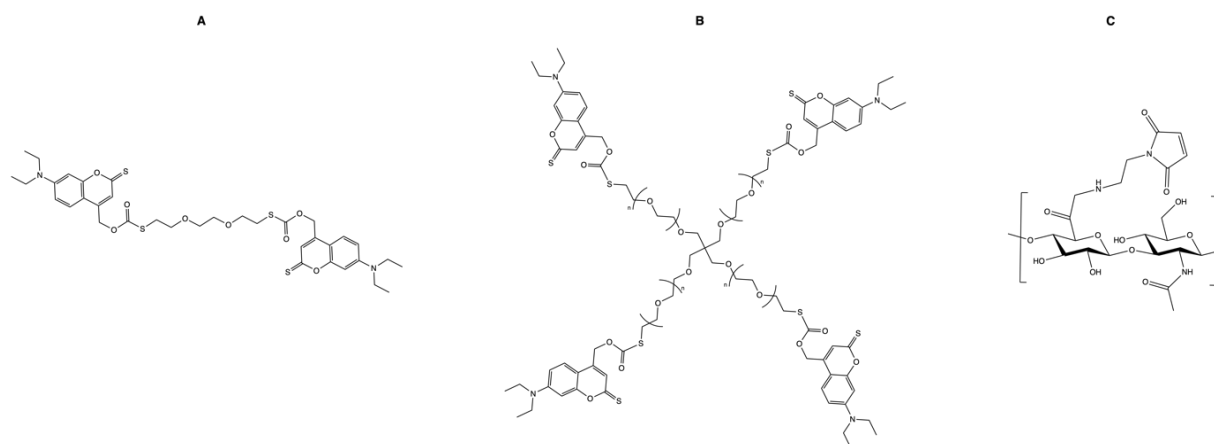

Figure 10: A: HA-MAL. B: Protected EDT. C: Protected 4arm PEG.

The PPG (*compound **6***) was synthesized from 7-Diethylamino-4-methylcoumarin in six synthesis steps. The synthesis route and the intermediary products are shown in Scheme 4.
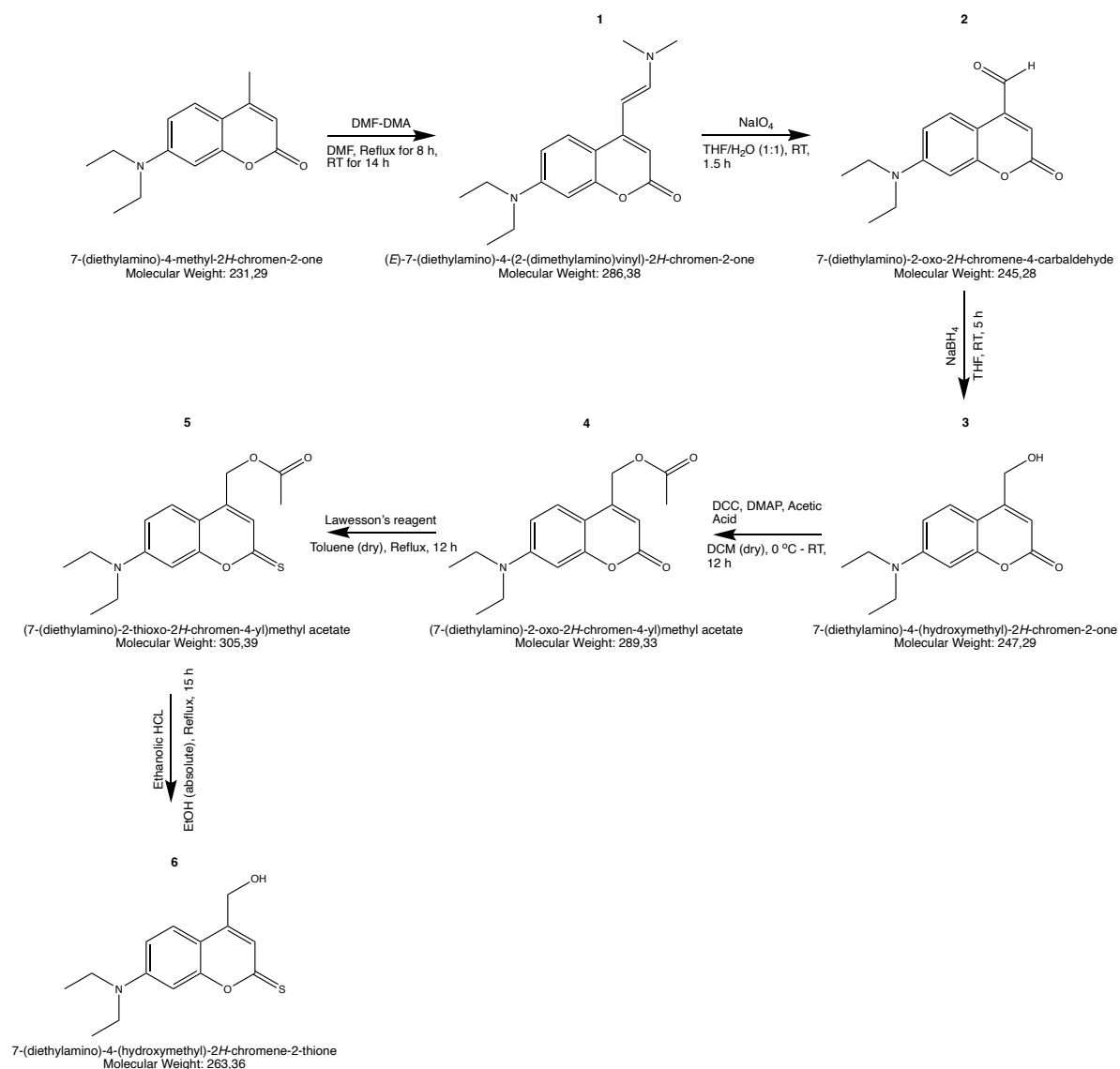
Scheme 4: Synthesis route of the photocleavable protecting group (compound **6**).

2.2.2 Absorbance spectra

*Compounds **3**, **6**,* and *protected EDT* were dissolved in ACN/PBS (1:1). *Protected 4arm PEG* was dissolved in PBS only. Partial solvation was observed by a color change to yellow, whilst some solid particles remained present. Further dilution to respective concentrations of 0.36 mM, 0.21 mM, 0.59 mM, and 0.686 μM was done to not exceed absorbance measurability. In a 96 flat-bottom well plate, three wells were filled with 0.2 mL for each sample and the blank. Empty rows were kept in between the sample rows to prevent sample interference. Absorbance spectra were measured between 310 and 710 nm. Unless stated otherwise, all absorbance spectra were measured using a CLARIOstar plus with MARS Data Analysis Software. Both were obtained from BMG LABTECH, Germany.

HA-MAL (12% DoF) was dissolved in 10x PBS to a 1% w/w solution. In a 96 flat-bottom well plate, three wells were filled with 0.1 mL for both the sample and the blank, with an empty row in between. For 76 hours, absorbance spectra were measured between 250 and 700 nm.

For calculation of the molar extinction coefficient (ε), calibration series were made in ACN/PBS (1:1) of compound 6 and protected 4arm PEG. Respective stocks of 0.1 mg/mL ($3.8*10^{-4}$ M) and 0.25 mg/mL ($4.1*10^{-5}$ M) were made. Compound 6 dilution series consisted of 0.075, 0.05, 0.025, 0.02, 0.02, 0.005, 0.0025 mg/mL ($2.84*10^{-4}$, $1.9*10^{-4}$, $9.5*10^{-5}$, $7.6*10^{-5}$, $3.8*10^{-5}$, $1.9*10^{-5}$, $9.5*10^{-6}$ M). Protected 4arm PEG dilution series consisted of 0.25, 0.125, 0.0625, 0.025 mg/mL ($4.1*10^{-5}$, $2.1*10^{-5}$, $1.0*10^{-5}$, $4.1*10^{-6}$ M). Absorbance spectra were measured in triplicate between 350 and 700 nm by a Shimadzu UV-2400PC Series, obtained from the Shimadzu Corporation, Japan. Measurement properties were as follows: medium scan speed, 0.2 nm sampling interval with auto sampling interval enabled, 1 nm slit width, normal S/R exchange, 0.0001 operation threshold with 4 points. Quartz cuvettes with a 1 cm path length were used in a 6-cell holder.

2.2.3 Calculation transmittance and molar extinction coefficient

The molar extinction coefficient (ε) can be calculated with the absorbance (A), concentration (c), and path length (l), according to the Lambert-Beer law:

$$A = \varepsilon * c * l. \tag{1}$$

Absorbance limits VBP printability. Considering a minimum needed light transmittance, absorbance (A) can be calculated with the ratio of starting intensity (I_o) and intensity after transmittance (I_T), according to the formula:

$$A = \log_{10} I_0 / I_T. \tag{2}$$

First, ε was calculated first by absorbance of *protected 4arm PEG* in known concentrations, and path length, using formula (*1*). Second, assuming at least 37% transmittance is needed in the volumetric bioprinter, absorbance was calculated setting intensity after transmission to 37% and starting intensity to 100%, using formula (*2*). Third, the calculated absorbance was used to calculate concentration using formula (*1*).

2.2.4 Statistical analyses

One-way ANOVA using GraphPad Prism version 9.5.0 for Mac was performed. It was obtained from GraphPad Software, USA.

2.2.5 NMR experiments

After measuring 1% *HA-MAL* (12% DoF) absorbance spectra, the remaining stock solution was freeze-dried after 76 hours. Then, the dry powder was redissolved in D_2O and ^1H NMR was measured to confirm maleimide degradation.

To confirm maleimide-thiol conjugation, *linear PEG* and *EDT* dissolved together and analyzed by ^1H NMR. Two standards and two samples were made. Standard 1 contained 9.9 mg *linear PEG 2 kDa* in 1 mL PBS. Standard 2 contained 9.9 mg *linear PEG 5 kDa* in 1 mL PBS. Sample 1 contained 10.7 mg *linear PEG 2 kDa*, and 9.1 mg *EDT* (10 eq) in 1 mL PBS. Sample 2 contained 10.1 mg *linear PEG 5 kDa* and 3.6 mg *EDT* (10 eq) in 1 mL PBS. After reacting for 1 hour, samples were frozen at -80 ºC for 30 minutes and freeze-dried. Dried samples were

redissolved in D₂O and put in incubator at 37 °C for 30 min. After solvation, ¹H NMR measurements were done.

2.2.6   GPC experiments

As the degree of *linear PEG* conjugation to *EDT*, shown in Scheme 5, is positively correlated to polymer size, GPC was performed.
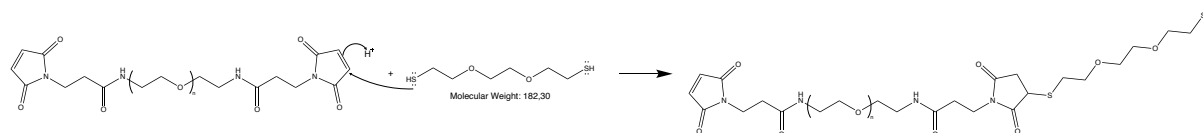
Scheme 5: Linear PEG conjugation to EDT by means of the thiol-ene mechanism.

GPC was done in DMF containing 10 mM LiCl. Since the thiol-ene reaction may occur in both PBS and DMF, two sample groups were created. In the first sample group, *linear PEG 2 kDa* and *linear PEG 5 kDa* were allowed to react to *EDT* in PBS for one hour, at a molar ratio of 0.0015 M and 0.0006 M, respectively. The reason for the molar difference being that the system has an optimal detection ability for samples that contain 3 mg/mL of compound.

Four samples were prepared, each in triplicate. Stock solutions were prepared by dissolving the *linear PEGs* and *EDT* in PBS. From these stocks, two standards (only the *linear PEGs*) and two samples (*linear PEGs* and *EDT*) were prepared (Table 2), 1 mL each. After one hour at room temperature, samples were frozen at -80 °C for 30 min. Samples were freeze-dried and redissolved in 1 mL DMF containing 10 mM LiCl. Some precipitate was visible. The samples were incubated at 37 °C for 30 min. Further solvation was allowed overnight. Then, samples were centrifuged at 7000 rpm for 2 min., and the supernatant was transferred into a filter GPC vial. In the second sample group, the *linear PEGs* were allowed to react to EDT in DMF containing 10 mM LiCl directly. Four samples were prepared in the same molar ratios and component conditions as the first group (Table 2), except for freezing, freeze-drying, and centrifuging. No precipitate was visible in the second group.

Table 2: Sample set-up for conjugation assessment by GPC.

Condition	Sample	EDT	Linear PEG 2000	Linear PEG 5000
PBS → DMF	Standard 1		✓	
	Standard 2			✓
	1	✓	✓	
	2	✓		✓
DMF	Standard 1		✓	
	Standard 2			✓
	3	✓	✓	
	4	✓		✓

Using as solvent DMF with 10 mM LiCl added, the measurement protocol included a flow rate set to 1 mL/h, column temperature to 65 °C, and UV measurements at 214 and 280 nm. Measurements were done using an Alliance e2695 separations module with a mixed-D column, connected to a 2414 Refractive Index (RI) detector and UV 2489 UV/Vis detector. Empower 3 was used for data analysis. All were obtained from the Waters Corporation, USA.

2.2.7 Hydrogel preparations

2.2.7.1 Linear PEG 2 kDa and 4arm PEG test concentrations

Hydrogels were created by mixing *linear PEG 2 kDa* and *4arm PEG*. Keeping the ratio of maleimide to thiol to 1:1, decreasing weight percentages were tested for hydrogel formation in PBS. Hydrogels decreasing from 4.5% to 1% (w/w) were made by mixing 0.1 mL of stock solutions in PBS in a 1:1 ratio, resulting in average concentrations (w/w) of both components, shown in Table 3.

Table 3: Sample overview of linear PEG and 4arm PEG hydrogel formation in decreasing concentrations. To be noted is that the molar ratios are 1:2 for linear PEG and 4arm PEG, resulting in a 1:1 maleimide and thiol ratio.

Final Weight percentage	Linear PEG stock concentration		4arm PEG stock concentration	
	(mmol/mL)	(mg/mL)	(mmol/mL)	(mg/mL)
4.5 %	0.0198	40	0.0099	50
3%	0.0132	27	0.0066	33
2%	0.0088	18	0.0044	22
1.5%	0.0066	13.2	0.0033	16.5
1%	0.0044	8.8	0.0022	11

2.2.7.2 Linear PEG 2 kDa and protected 4arm PEG

When using the *protected 4arm PEG* its higher molecular weight was taken into consideration compared to the unprotected *4arm PEG* to create 3% (w/w) hydrogels. The *protected 4arm PEG* did not dissolve completely. Nevertheless, they were mixed 1:1, taking 0.1 mL of each into clear glass vials. Three samples were prepared and irradiated through the vials, two were irradiated by visible light using a floodlight. Unless stated otherwise, all floodlight irradiations were done with a Jobmate IP65 20W LED floodlight, obtained from Jobmate, Australia. The remaining sample was irradiated by green light from a laser source at 473 nm. Unless stated otherwise, all specific wavelength irradiations were done by a Tomolite V2 volumetric bioprinter, obtained from Readily3D, Switzerland. Afterwards, samples were visually compared to the 3% (w/w) with the unprotected *4arm PEG*, yielding the test conditions in Table 4.

Table 4: Hydrogel formation of linear PEG 2 kDa and protected 4arm PEG under various conditions.

Sample	Light source	Irradiation time (min)	Notes
A	None	0	Control
B	Floodlight	3	Showed increased viscosity after 10-20 seconds.
C	Floodlight	3	Similar as sample *B*.
D	Laser	3	Direct control was used to irradiate the whole solution and the plateau was rotated a few times. After 30 seconds, a better gel seemed to have formed already than samples *B* and *C*.

2.2.7.3 Increasing solubility of protected 4arm

The remainder of the stock sample of *protected 4arm PEG* that was used to make the samples of Table 4 was sonicated for 30 minutes at 40 °C, without improvement.

Two 3% (w/w) hydrogels with *linear PEG 2 kDa* and *protected 4arm PEG* were prepared to include 5% DMSO (A) and 50% ACN (B). To improve solvation, stock solutions were bypassed. Linear PEG was dissolved first in solvents A and B in the final volume at 1.3% (w/w). The dissolved linear PEG in the final volume was then added to the protected PEG to 3% (w/w) solutions. Samples were transferred to clear glass vials and irradiated by a floodlight for 3 minutes.

2.2.7.4 HA-MAL and 4arm PEG test concentrations

Hydrogels were created by mixing solutions of *HA-MAL* (12% DoF) and *4arm PEG*, shown in Table 5. Concentrated stock solutions of *HA-MAL* and *4arm PEG* were prepared in 10x PBS. They were added separately to a volume of 10x PBS needed to obtain the final concentrations and mixed. One sample was prepared using 1x PBS only, with the final pH measured at 4. The final pH of other samples was measured at 7.

Table 5: Sample overview of HA-MAL and 4arm PEG hydrogel formation in decreasing concentration. [a]Maleimide concentration of HA-MAL. [b]Thiol concentration. [c]Prepared in duplicate, using only 10x PBS or only 1x PBS respectively.

Sample	HA-MAL concentration			4arm PEG concentration		
	(mmol/mL)[a]	(mg/mL)	Percentage (w/w)	(mmol/mL)[b]	(mg/mL)	Percentage (w/w)
1[c]	0.0030	10	1	0.0040	5	0.5
2	0.0018	6	0.6	0.0024	3	0.3
3	0.0015	5	0.5	0.0020	2.5	0.25
4	0.0012	4	0.4	0.0016	2	0.2
5	0.0009	3	0.3	0.0012	1.5	0.15
6	0.0006	2	0.2	0.0008	1	0.1

2.2.7.5 HA-MAL and protected 4arm PEG

Subsequently, only 10x PBS was used in four samples, using *HA-MAL* (12% DoF).

Sample 1 was prepared from *HA-MAL* and protected 4arm PEG. A 1% (w/w) *HA-MAL* solution was added to *protected 4arm PEG* to obtain respective concentrations of 1% and 0.5% (w/w). The pH was measured at 7. Solvation was not complete. Sample was centrifuged at 6000 rpm for 5 minutes, and 0.2 mL of supernatant was transferred to a clear glass vial. It was put under a floodlight for 3 minutes.

Sample 2 was prepared from *HA-MAL* and a combination of *4arm PEG* and *protected 4arm PEG*. *HA-MAL* was dissolved at 0.6% first. Secondly, this solution was added to *4arm PEG*, obtaining a 0.6% *HA-MAL* and 0.15% *4arm PEG* solution. Thirdly, the solution was added to *protected 4arm PEG*, yielding a final solution with 0.6% *HA-MAL*, 0.15% *4arm PEG*, and 0.15% *protected 4arm PEG*. Despite the low concentration of *protected PEG*, solvation was not complete. The sample was centrifuged at 6000 rpm for 5 min, 0.3 mL of the supernatant was transferred to a clear glass vial and irradiated using 473 nm. Direct control was used to

irradiate the whole solution for 30 seconds with, whilst rotating. After hydrogel formation, 0.5 mL PBS was added to see if the hydrogel remained.

Sample 3 was prepared from *HA-MAL* and *protected 4arm PEG*. *4arm PEG* was dissolved at 0.12% (w/w). The solution was then added to *HA-MAL* for addition of 0.6% (w/w) to the solution. The solution was then added to *protected 4arm PEG* for addition of 0.2% (w/w), yielding a final solution of 0.6% *HA-MAL*, 0.12% *4arm PEG*, and 0.2% *protected PEG*. Solvation was not complete. The sample was filtrated through a 0.45 μm, the filter became dark yellow, the filtrate was light yellow. 0.3 mL of the filtrate was transferred to a clear glass vial and irradiated using 520 nm. Direct control was used to irradiate the whole solution, whilst rotating. The total duration was 7 minutes.

Sample 4 was prepared from *HA-MAL* and *protected 4arm PEG*. *HA-MAL* was dissolved in first at 1.2% (w/w). *Protected 4arm PEG* was dissolved in at 0.6% (w/w), put in incubator at 37 $^{\circ}$C for 15 minutes. Despite incomplete solvation, both solutions were mixed in a 1:1 ratio, yielding a 0.6% *HA-MAL* and 0.3% *protected 4arm PEG* solution. No difference was observed after keeping overnight in the dark, to allow for longer solvation. 0.3 mL of the solution was transferred to a clear glass vial and irradiated using 520 nm. Direct control was used to irradiate the whole solution, whilst rotating. The total light exposure duration was 7 minutes, with hydrogel formation observed after 5 minutes.

3　Results and Discussion

3.1　Synthesis

Respective synthesis yields for *compounds 1 to 6*, shown in Scheme 6, were 66% ±6.3% (n=4), 93% ±19.6% (n=5), 92% ±4.1% (n=4), 87% ±4.5% (n=3), 49% ±7% (n=4), 83% ±5.8% (n=4). For *compound 6*, before method optimization, yields of 20%, 22.4%, 46%, 49%, and 63% were obtained.
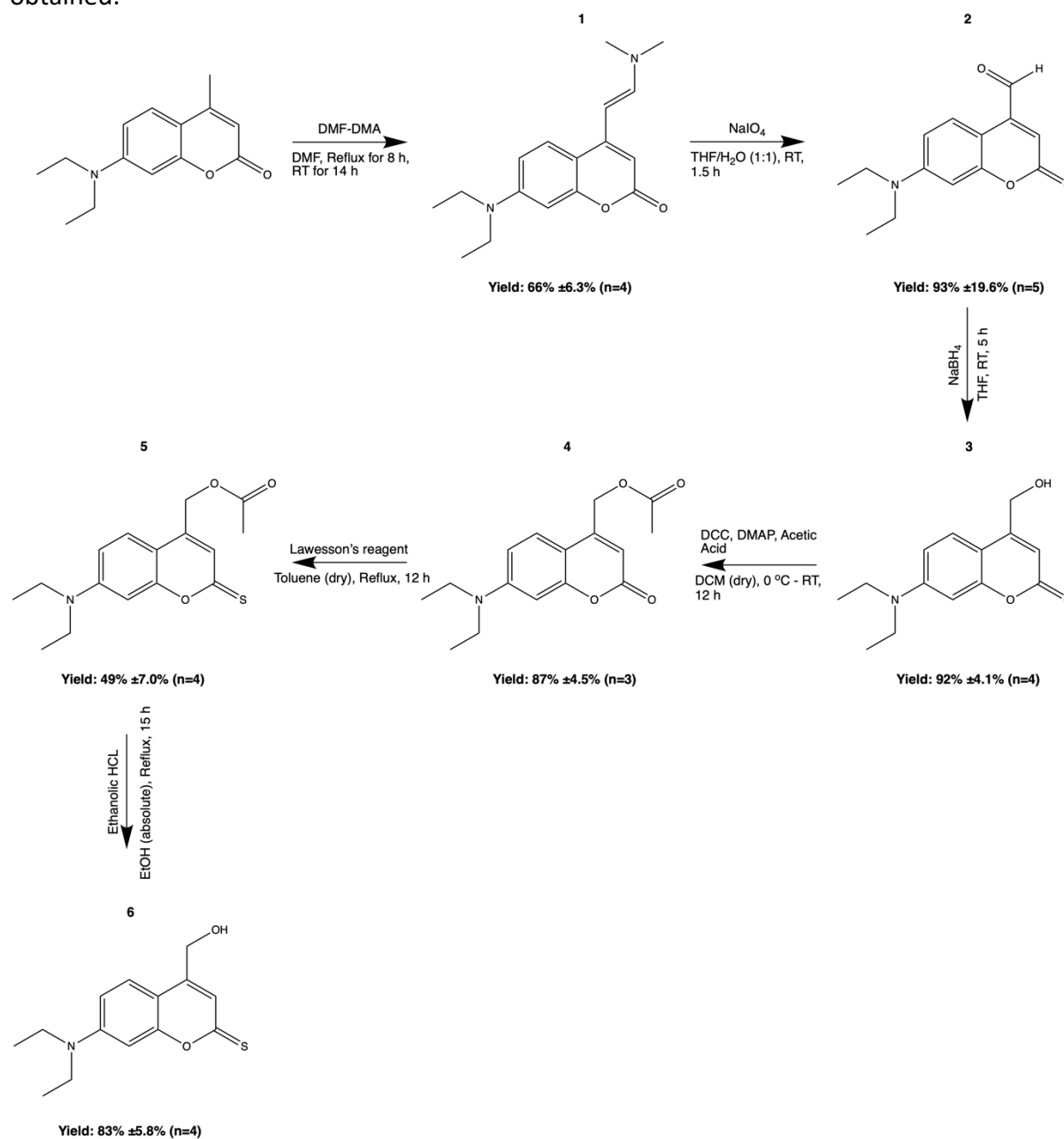
Scheme 6: Yield results for PPG and intermediary compounds.

Respective synthesis yields for *protected EDT* and *4arm PEG* were 100% (n=1) and 78% ±10% (n=2), shown in Scheme 7 and Scheme 8. Degrees of protection for *EDT* and *4arm PEG* were 100% (n=1) and 80% ±0% (n=2), respectively.
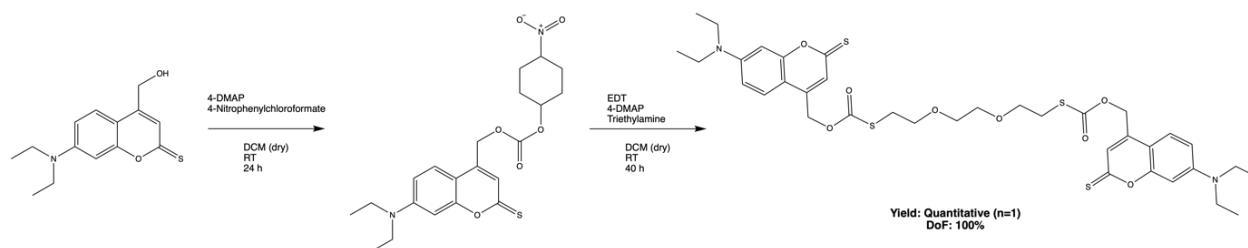
Scheme 7: Yield and DoF results for protected EDT synthesis.
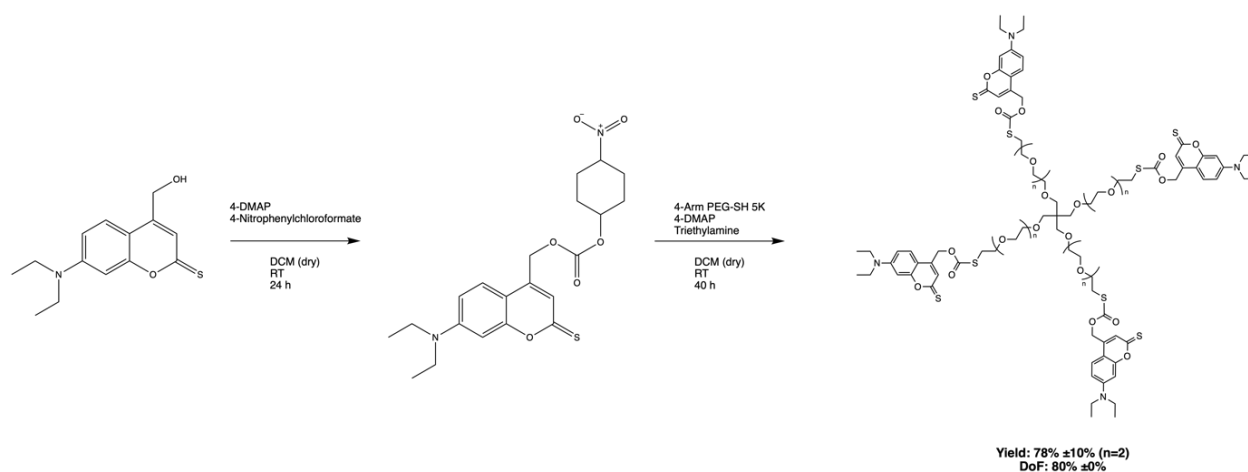
Scheme 8: Yield and DoF results for protected 4arm PEG synthesis.

HA-MAL was synthesized quantitatively (n=2), with degrees of protection of 12% and 6.5%, shown in Scheme 9.
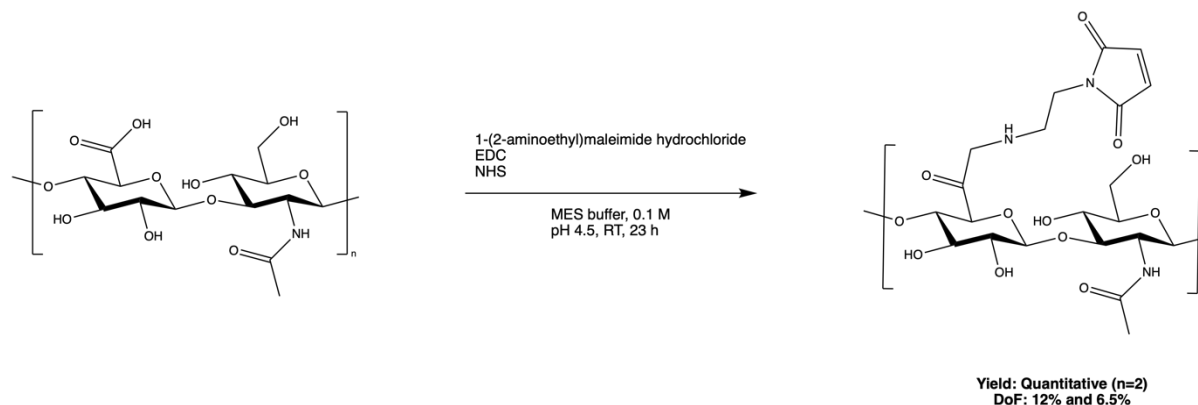
Scheme 9: Yield and DoF results for HA-MAL synthesis.

3.1.1 Considerations

Yields were somewhat different compared to the yields obtained in the articles from which the synthesis protocols were used or adjusted, shown in Table 6 and Figure 11.

Table 6: Overview of achieved yields of each reaction compared to reference protocols. ª: Purification of compound 6 was improved. Only the yield of the improved method is listed.

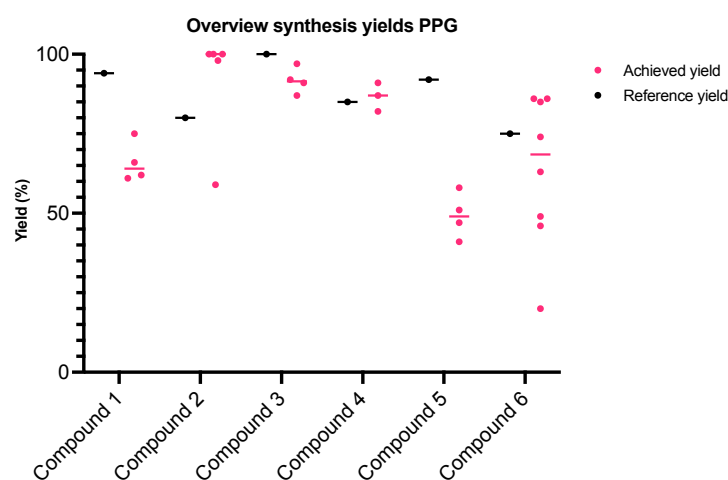| Component	Original yield	Achieved yield (s, n)	Protection/ functionalization
Compound 1	94%[78]	66% (6.3%, 4)	
Compound 2	80%[79]	93% (19.6%, 5)	
Compound 3	*Quantitative*[79]	92% (4.1%, 4)	
Compound 4	85%[65]	87% (4.5%, 3)	
Compound 5	92%[65]	49% (7.0%, 4)	
Compound 6	75%[65]	83% (5.8%, 4)[a]	
Protected EDT	N.A.	*Quantitative* (0, 1)	100%
Protected 4arm PEG-SH 5 kDa	N.A.	78% (10.0%, 2)	80%
HA-MAL	N.A.	*Quantitative* (0, 2)	12%, 6.5%

Figure 11: Achieved yields of each synthesis reaction compared to the yield achieved in the protocol used as a reference. For compound 6, all syntheses are shown (n=8).

The lower yield of *compound 1* may be explained by a tenfold smaller scale compared to the synthesis of Klimek *et al.*[78] When using a filter of the same size, the amount of compound staying inside the filter does not increase up to a certain point when upscaling. This means that on a smaller scale, relatively more compound is lost. Besides, Klimek *et al.*[78] did not specify the volume of ice water to which the precipitate should be added. The used volume may have been different, influencing the size and shape of the precipitated crystals. Larger formed crystals would have made purification easier and likely increased the yield. Shown in the Supporting Information, the small $-CH_3$ peak at 2.3 ppm of the ^1H NMR spectrum of the base compound (Figure S4) remained present (Figure S5), indicating that conversion was not 100% and the actual yield is slightly lower.

For *compounds 2 to 4*, synthesis in this thesis differed primarily from the original protocols in the method of purification of the synthesis. In the referenced protocols, two-phase extractions were followed by a final silica chromatography column, which was not done in the syntheses of these compounds for this thesis. An average yield of 91% for these compounds was obtained compared to an 88% average yield in the reference articles, despite the much smaller scale. Although some presence of the base compound remained until *compound 4* (-

CH$_3$ peak at 2.3 ppm, Figure S6-S8 of Supporting Information), yields are representative as the reaction mechanisms during syntheses of *compound 2* to *compound 4* are unreactive to the base compound.

However, Lawesson's reagent used for synthesis of *compound 5* is reactive to the base compound, which in part explains the lower average yield of 49% compared to the 92% in the reference article. Also, the omittance of chromatography after each intermediate synthesis explains why more impurities were present, lowering the yield. However, as the NMR spectra showed only minor impurities, *compounds 1* to *4* were deemed acceptable to use in follow-up reactions. This proves that silica column chromatography is not a necessity for intermediate compounds.

An additional explanation for the 49% yield of *compound 5* is that during this synthesis, the starting compound was not entirely dry (Supporting Information, Chapter S1.6). This means that the weights used for yield calculations may have been not entirely correct. Although trace amounts of acetone should not be an issue in all other syntheses, Lawesson's reagent is able to react with acetone, as it is a carbonyl, same as *compound 4* and the base compound. Thus, the available molar equivalent of Lawesson's reagent to *compound 4* may have been somewhat lower than intended. A simple solution would be to increase the amount of Lawesson's reagent to compensate for the change in reaction kinetics.

For *compound 6*, the silica column chromatography method in this thesis was improved compared to the referenced protocol, where first elution was done with DCM only and later with a 95 to 5 ratio of DCM/acetone, giving a 75% yield. Repetition of this protocol proved very difficult, with achieved yields between 20% and 63%. Shown in this thesis, dry loading instead of wet loading and the adjustment of gradually increasing acetone concentration to higher acetone concentrations up to a 50 to 50 ratio in the eluent gave an average yield of 83%. Although not listed, it is likely that this increases elution speed, decreasing the amount of needed solvent.

Although purification of modified PEG is commonly done by precipitation, for example with ether,[80] it is less useful for *protected 4arm PEG*. Especially if the protection mechanism is not 100% successful. If the DoF is lower than 100%, both the unprotected and protected PEG will be in the precipitate. This is undesirable as this will need to be considered when using it to make hydrogels.

The difference in *HA-MAL* yield may be explained by the stability of the coupling agent EDC in MES buffer solutions at low pH. In MES buffers EDC is stable at pH 7 at room temperature, with a half-life of 37 hours.[81] It was found that decreasing pH to respectively 6 and 5 decreases the half-life to 20 and 3.9 hours.[81] It is likely that in the MES buffer solution at pH 4.5 used here, EDC half-life was below 3.9 hours. As the difference between the two syntheses was that EDC and NHS were dissolved either immediately or 30 minutes before adding to the reaction mixture, the difference in yield can be explained by partial degradation of EDC in the latter case. Thus, it is recommended to dissolve EDC and NHS only briefly before adding to the reaction mixture.

3.2 Material quantification

3.2.1 Absorbance of PPG and conjugates

For c*ompound 3*, λ_{max} was found at 380 nm in ACN/PBS. For *compounds 6, protected EDT, and protected 4arm PEG,* λ_{max} was found near 470 nm in ACN/PBS. For *protected 4arm PEG* in only PBS, λ_{max} was 475 nm. Absorbance spectra of protective groups and protected PEG are shown in Figure 12.
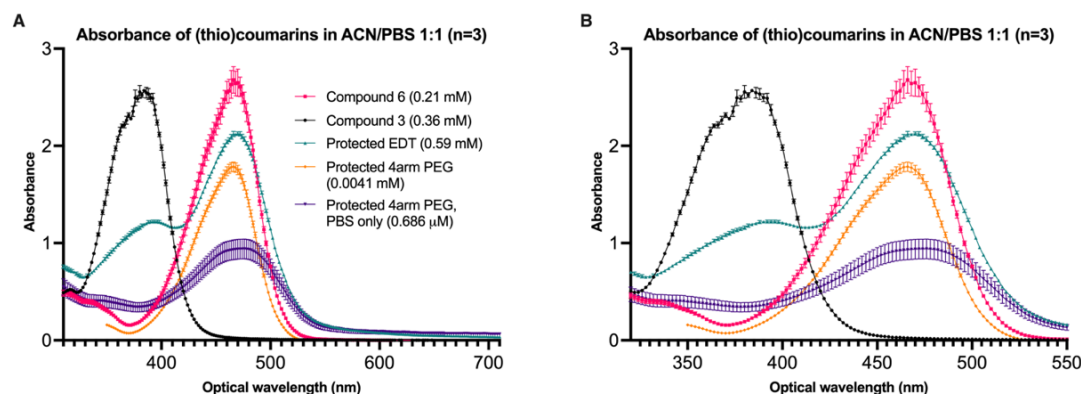

Figure 12: A: Absorbance spectra of compound 3, compound 6, protected EDT, and protected 4arm PEG. λ_{max} is ± 470 nm. B: Zoomed in.

An ε of 16956 $M^{-1}cm^{-1}$ was determined for *compound 6*, similar to the value found by Klimek *et al*. of 16500 $M^{-1}cm^{-1}$.[78] Of protected 4arm PEG, it was determined at 32392 (s=170, n=3) $M^{-1}cm^{-1}$ based on its calibration curve, or 39313 (s=1651, n=3) $M^{-1}cm^{-1}$ based on the triplicate sample. The molar amount of *compound 6* in the conjugated *protected 4arm PEG* was considered as well for 80% protection illustrated in Figure 13.
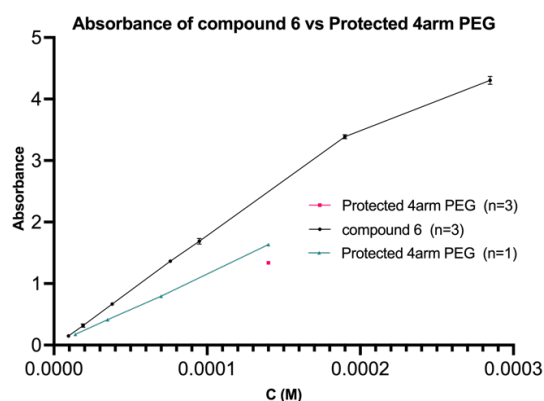
Figure 13: Absorbance at $\lambda=473$ nm of compound 6 and protected 4arm PEG corrected for the molar concentration of compound 6. For compound 6, an ε of 16965 (±1142) $M^{-1}cm^{-1}$ was calculated. For the protected 4arm PEG they were 32392 (±170, triplicate sample) and 39313 (±1651, calibration curve) $M^{-1}cm^{-1}$.

3.2.1.1 Considerations

It is preferable to have all absorbance spectra in PBS, as it is the medium intended to use when printing. It was not possible to obtain these data due to low solubility of shown compounds, except for the protected 4arm PEG. Interestingly, the difference in λ_{max} of both protected 4arm spectra (Figure 12) indicates a bathochromic shift, as λ_{max} increased with increasing solvent polarity. Thus, other shown compounds possibly have a similar bathochromic shift, resulting in a higher λ_{max} in PBS.

It was expected that the molar extinction coefficient of *protected 4arm PEG* was linearly correlated to the degree of protection. Considering 80% protection, the molar extinction coefficient was expected to be $0.8 * 4 * \varepsilon_{compound\ 6} \approx 54288$ M^{-1}cm^{-1}. However, the actual value was much lower at 32392-39313 M^{-1}cm^{-1}. The implication is that the absorbing character of *compound 6* is different in free form compared to its conjugated form. This is also in line with the slightly different respective shapes of the absorbance spectra (Figure 12). The data here suggests that *compound 6* decreases in absorbance when it is conjugated to *4arm PEG* (Figure 13). One reason for this may involve changed binding energies. During absorbance, atomic electrons are liberated from atoms due to photons losing their entire energy to them.[82] For this to occur, the energy of a photon needs to be higher than the binding energy of that particular electron. It is possible that because of conjugation of *compound 6* to *4arm PEG* the binding energies of electrons involved in absorbance have changed. Another factor may be that particle distribution of *compound 6* may be different in free form compared to its conjugate. In free form, molecules are uniformly distributed when dissolved, but when conjugated, they are clustered together on *4arm PEG*, which are uniformly distributed themselves when dissolved. Therefore, interaction kinetics between photons and *compound 6* may be different.

3.2.2 HA-MAL quantification

Maleimide absorbance decreased to 50% after 20 hours, although the decline is nonlinear. Significant decreases were found between time points 0.2-2 h (****), 2-5 h (***), 5-22 h (****), 25.5-46 h (***), and 46-69 h (***). Absorbance of *HA-MAL* over time is shown in Figure 14. Spectra at various time points are shown (*A, B*), and the absorbance at 296 nm was compared in time (*C, D*).

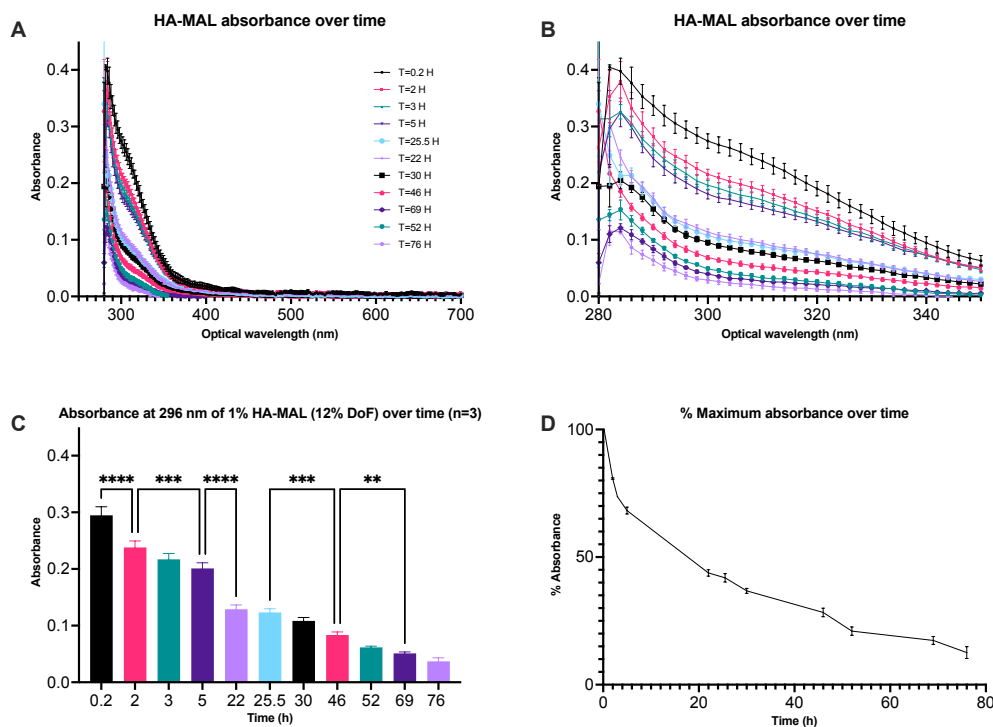*Figure 14: A: 1% HA-MAL maleimide absorbance over time, n=3. B: Zoomed in between 280 and 350 nm. C: Decrease in 1% HA-MAL (12% DoF) absorbance at λ=296 nm over time. ** p ≤0.01, *** p ≤0.001, **** p ≤0.0001, n=3. D: Absorbance expressed as percentage from start. Time point at 0.2 h was assumed to be 100%.*

Maleimide protons at the -ene are visible at 6.9 ppm, with an integer of 0.24. After 76 h, the peaks at 6.9 ppm are absent, with the integer of 0.01. New peaks are present at 6.0 and 6.3 ppm, with a combined integer of 0.23. Full spectra are shown in Figure 15.
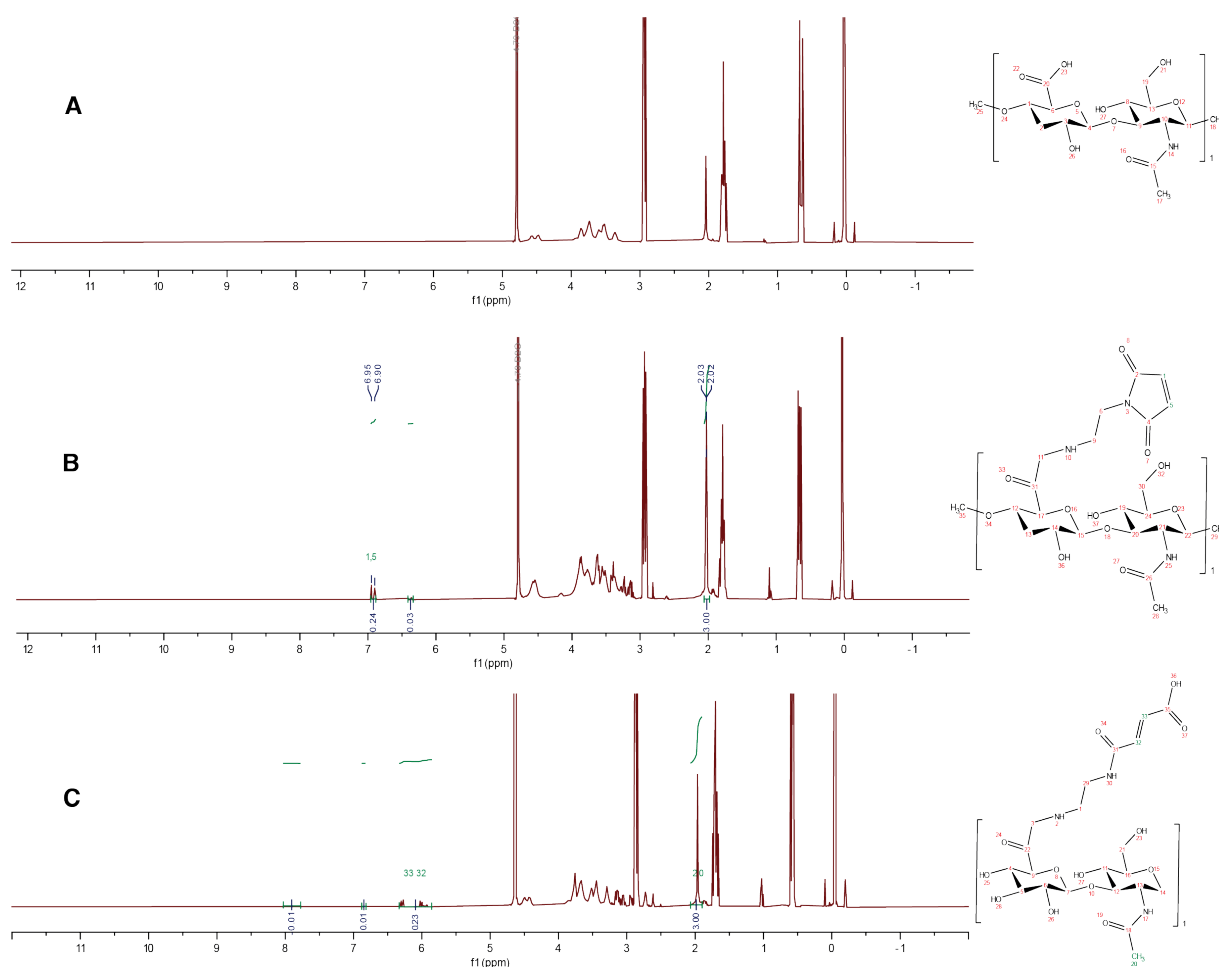
Figure 15: ¹H NMR visualization of the shift of the protons on the -ene before and after synthesis, and after maleimide degradation. A: HA before maleimide functionalization. B: HA-MAL. Peaks at 6.9 ppm have been attributed to protons on C1 and C5. C: HA-Maleic acid. Peaks at 6.0 and 6.3 ppm have been attributed to protons on C32 and C33.

3.2.3   Considering maleimide degradation in print sample preparation

The implication of maleimide degradation for VBP is that *HA-MAL* needs to be used within a short timeframe after preparation. The reason is that the -ene of the maleimide is far more reactive than that of maleic acid. Whereas maleimide shows full conjugation to thiol without catalyst within a minute,[80] maleic acid and other linear -enes conjugate slower, even in the presence of catalysts or initiators.[73,83] Maleimide degradation after conjugation will not be a problem as the covalent bond will still be present, illustrated in Scheme 10. The pH sensitivity follows from the hydroxide ions being the reactants: at lower pH their concentrations are very low.
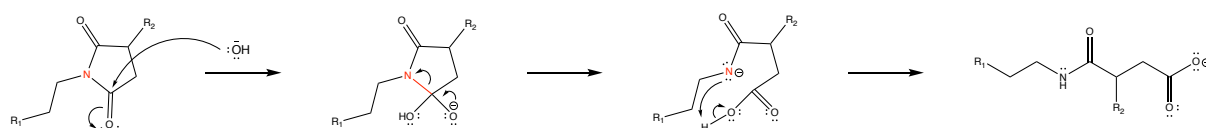
Scheme 10: Despite maleimide degradation into maleic acid, cross-links between HA-MAL (R1) and 4arm PEG (R2) remain.

3.3 Thiol-maleimide conjugation

3.3.1 NMR

Shown in Figure 16 and Figure 17 are NMR spectra before and after thiol-maleimide conjugation.

Figure 16: PEG 2 kDa (MAL)2 - EDT conjugation. A: The number of protons of the repeating PEG unit at 3.7-3.8 ppm was set at 182. The protons of the maleimide -ene at 6.9 ppm, integrated at 2.56 protons (should be 4). B: Thiol-ene conjugation of all maleimides results in absence of the -ene peak at 6.9 ppm and yields a new peak at 2.77 ppm of the resulting -CH₂ on the maleimide. Integrations yields an estimation of 3.2 protons (should be 4). C: A, zoomed in. D: B, zoomed in.

Figure 17: PEG 5 kDa (MAL)2 - EDT conjugation. A: The number of protons of the repeating PEG unit at 3.7-3.8 ppm was set at 454. The protons of the maleimide -ene at 6.9 ppm, integrated at 2.56 protons (should be 4). B: Thiol-ene conjugation of all maleimides results in absence of the -ene peak at 6.9 ppm and yields a new peak at 2.77 ppm of the resulting -CH$_2$ on the maleimide. Integrations yields an estimation of 3.97 protons (should be 4). C: A, zoomed in. D: B, zoomed in.

Before thiol-maleimide conjugation of linear PEG 2 kDa and EDT, two -CH groups of the maleimide were visible at 6.9 ppm. Setting the integer of the PEG protons at 3.7 ppm at 182 protons yielded an integer of 2.56 protons at 6.9 ppm. After conjugation, the peak at 6.9 ppm disappeared and a new peak of the -CH$_2$ groups of the former maleimides appeared at 2.77 ppm, integrated at 3.2 ppm. For linear PEG 5 kDa and EDT, two -CH groups of the maleimide were visible at 6.9 ppm. Setting the integer of the PEG protons at 3.7 at 454 protons also yielded an integer of 2.56 protons at 6.9 ppm. After conjugation, the peak at 6.9 ppm disappeared and a new peak appeared at 2.77 ppm, integrated at 3.97 protons.

Although the conjugation is clearly visible, NMR does not provide information about the final particle size, since both linear PEGs and EDT have their reactive groups on both ends. Studying particle size may give an insight into cross-linking kinetics, as larger particle size indicates higher reaction rate. This is because as conjugated complexes form, the molar concentrations of unconjugated molecules decrease.

3.3.2 PEG-MAL GPC

Conjugation particle size is shown in Figure 18. For full spectra, see Supporting Information, chapter S3. For samples first reacted in PBS, standard particle size was measured at 2589.3 ±53.1 Da for linear PEG 2 kDa, and 5886.3 ±84.0 for linear PEG 5 kDa. Conjugated samples showed 3 populations (P1, P2, P3). Linear PEG 2 kDa and EDT yielded populations of 2543.7 ±8.0, 5543.3 ±70.0, and 9085.7 ±16.6 Da. Linear PEG 5 kDa and EDT yielded sizes of 5801.7 ±13.1, 12747.0 ±11.8, and 19983.7 ±22.0 Da (*A*). For samples dissolved directly in DMF, standard particle size was measured at 2619.7 ±48.8 Da for linear PEG 2 kDa, and 5947.7 ±63.8 Da for linear PEG 5 kDa. Linear PEG 2 kDa and EDT yielded populations of 1857 ±3.5 and 8416.3 ±1838.8 Da. Linear PEG 5 kDa and EDT yielded sizes of 4296.3 ±34.1, 19749.3 ±9480.6, and 48539.0 (s=0, n=1) Da (*B*). As for the fraction of each population in PBS, shown in (*C*), linear PEG 2 kDa and 5 kDa consisted of 100% P1. Linear PEG 2 kDa and EDT were 71.8% ±1.6% P1, 12.8% ±1.23% P2, and 15.41% ±0.9% P3. Linear PEG 5 kDa and EDT were 66.1% ±2.2% P1, 15.3% ±1.8% P2, 18.6% ±1.1% P3. As for fractional population size, shown in (*D*), linear PEG 2 kDa and 5 kDa consisted of 100% P1. Linear PEG 2 kDa and EDT were 32.5% ±2.6% P1, and 67.5% ±2.6% P3. Linear PEG 5 kDa and consisted of 23.6% ±3.9% P1, 13.3% (s=0, n=1) P2, 72% ±3.7% P3.
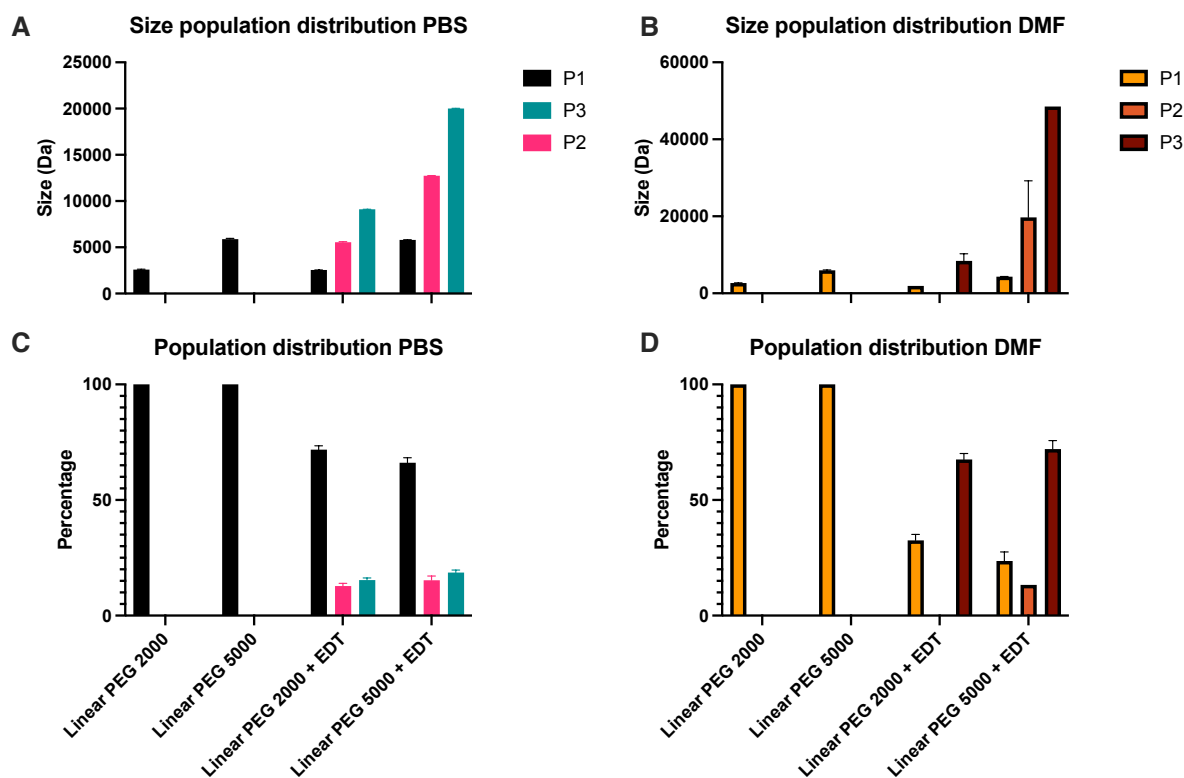
Figure 18: GPC size estimation of linear PEG and EDT conjugates (n=3). A: For samples first reacted in PBS, standard particle size was measured at 2589.3 Da (s=53.1) for linear PEG 2 kDa, and 5886.3 Da (s=84.0) for linear PEG 5 kDa. Linear PEG 2 kDa and EDT yielded populations of 2543.7 (s=8.0), 5543.3 (s=70), and 9085.7 (s=16.6) Da. Linear PEG 5 kDa and EDT yielded sizes of 5801.7 (s=13.1), 12747.0 (s=11.8), and 19983.7 (s=22) Da. B: Samples dissolved directly in DMF, linear PEG 2 kDa and 5 kDa standard particle size was measured respectively at 2619.7 Da (s=48.8) and 5947.7 Da (s=63.8). Linear PEG 2 kDa and EDT yielded populations of 1857 (s=3.5) and 8416.3 (s=1838.8) Da. Linear PEG 5 kDa and EDT yielded sizes of 4296.3 (s=34.1), 19749.3 (s=9480.6), and 48539.0 (s=0, n=1) Da. C: P1, P2, and P3 as fractions of total for samples first reacted in PBS. Linear PEG 2 kDa: 100% P1. Linear PEG 5 kDa: 100% P1. Linear PEG 2 kDa + EDT: 71.8% (s=1.6) P1, 12.8% (s=1.23) P2, 15.41% (s=0.9) P3. Linear PEG 5 kDa + EDT: 66.1% (s=2.2) P1, 15.3% (s=1.8) P2, 18.6% (s=1.1) P3. D: P1, P2, and P3 as fractions of total for samples dissolved directly in DMF. Linear PEG 2 kDa: 100% P1. Linear PEG 5 kDa: 100% P1. Linear PEG 2 kDa + EDT: 32.5% (s=2.6) P1, 67.5% (s=2.6) P3. Linear PEG 5 kDa + EDT: 23.6% (s=3.9) P1, 13.3% (s=0, n=1) P2, 72% (s=3.7) P3.

Measured particle sizes are different from what was expected. Beforehand it was expected to see larger particle size in samples that were allowed to react in PBS first before dissolution in the GPC eluent, DMF. The total reaction time for the PBS samples was longer than of the others. Also the increased polarity of water compared to DMF should have yielded larger particles, as reaction rate increased with higher solvent polarity.[84] The most likely explanation is that the centrifugation of the PBS samples sedimented larger conjugated particles. This would also explain why the percentages of unconjugated particles are lower in the PBS samples. Unfortunately, the centrifugation step is necessary if the reaction is to be tested in the solvent that is eventually used for printing, an aqueous buffer. The reason is that the used GPC column cannot be used with undissolved salts. Another reason may be the influence of the salts in PBS, absent in the DMF samples. In the presence of salts, the negatively charged thiolate (Scheme 3) will be shielded to an extent by the positively charged ions. Displacing these requires additional energy, thus lowering reaction kinetics.

This experiment could be adjusted to be repeated. Advised changes for better comparison are inclusion of PBS salts in all samples and to have similar centrifugation in all samples. The fact that the thiol-ene reaction occurs both in water and DMF the complexity of having to correct for the influence of the GPC eluent. To negate this, it would be better to use a GPC

column suitable for aqueous solutions. However, in our case, the necessity of this experiment for VBP can be questioned. If hydrogels are formed successfully, that already is a measure of sufficient cross-linking kinetics for the application of VBP.

3.4 Hydrogel formation by photocleavable mechanism

This chapter should be viewed as exploratory information, meant to obtain starting points on how to print with the protected 4arm PEG. Although not all results could be validated in triplicate due to time constraints, they are useful in determining which future directions can be taken on how to use these materials in VBP.

3.4.1 PEG based hydrogel formation

Hydrogel formation of *linear PEG 2 kDa* and *4arm PEG* at various concentrations (w/w percentage) is shown in Figure 19. Although hydrogel-like, the 1.5% and 2% (w/w) increased in viscosity only. After addition of 1 mL PBS to a 3% sample, the hydrogel remained for a few weeks, until discarded (not shown). The 2% and 1.5% (w/w) concentrations did not have this stability as they dissolved within multiple hours (not shown).
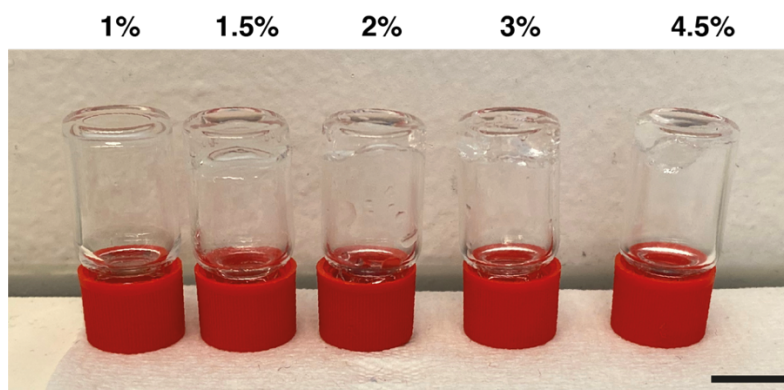

Figure 19: Hydrogel formation of linear PEG 2 kDa and 4arm PEG in PBS. Percentages are in w/w. Scale bar represents 10 mm.

When considering the lowest usable concentration, hydrogels should remain even after dilution. This is because when printing cells, liquid culture medium should be added after printing without changing the 3D shape of the construct. Of *linear PEG 2 kDa* and *4arm PEG* the minimum concentration is 3%. This corresponds to other hydrogel preparations using similar components[85] and also other 4arm PEGs and thiols.[86] The added benefit of using low concentrations is a lower cross-link density, facilitating higher cell density and higher expression of extracellular matrix genes.[87]

Hydrogel formation of the *linear PEG 2 kDa* and *protected 4arm PEG* is shown in Figure 20. The remaining stock solution of protected 4arm PEG became a hydrogel the next day (not shown). Samples B and C were bordering between a gel and a viscous fluid. Sample D is a hydrogel but did not appear as strong as the control.
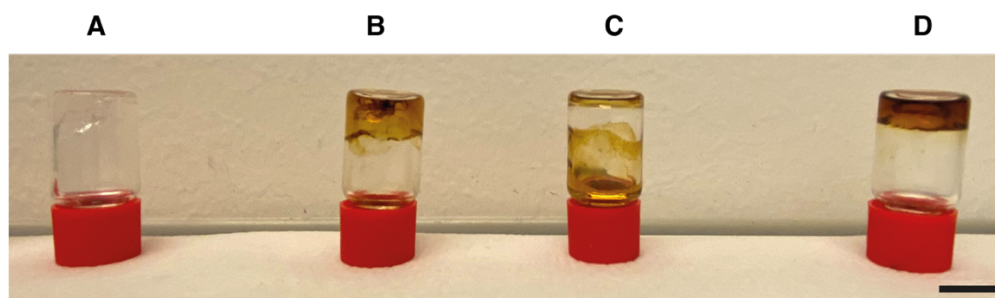
Figure 20: Hydrogel formation of linear PEG 2 kDa and protected 4arm PEG in PBS at 3% w/w. A: Control. B and C: Gel formation after floodlight irradiation, 3 minutes. D: Gel formation after laser irradiation (λ=473 nm), 3 minutes. Scale bar represents 10 mm.

The reason for less efficient cross-linking of samples using *protected 4arm PEG* compared to the control is worse dissolution. Since polar solvents are suggested to mediate photocleavage,[88] fewer water molecules interacting with *protected 4arm PEG* will make decoupling less energetically favorable. However, as demonstrated by sample D, this is counteracted when using a higher energy light source.

A practical consideration when working with stock solutions of *protected 4arm PEG* is storage in the dark and for limited time. This is because 4arm PEG can gel by itself as well due to the formation of disulfide bonds. The gelling of the remaining stock after a day indicates slow deprotection at normal lighting conditions.

Hydrogel formation using PBS with DMSO or ACN was unsuccessful. Also, the ACN/PBS sample was darker, shown in Figure 21.
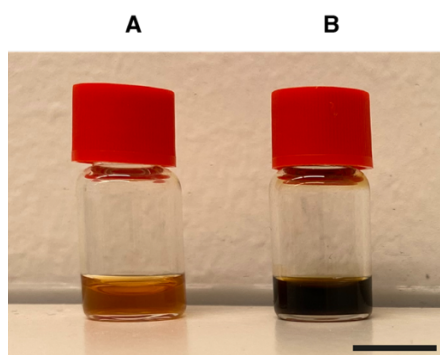
Figure 21: No hydrogel formation in linear PEG 2 kDa and 4arm PEG samples. A: 3% w/w in PBS with 5% DMSO. B: 3% w/w in PBS/ACN 1:1. Scale bar represents 10 mm.

The color difference may be due to the low water solubility of *compound 6* that is released after cleavage. Considering similar cleavage, the amount of released *compound 6* is similar in both vials, but the undissolved or precipitated amount will be higher in the more polar solution, A. During synthesis of *compound 6* it was seen that when concentrating it the color changed from yellow to a darker color.

The addition of organic solvents such as DMSO and ACN for complete dissolution does not seem desirable, as no hydrogels were formed. This observation can be explained by the increase in pKa of thiols in organic solvents. Relative to water, the pKa of thiols in general has been calculated to be higher by 3.7 and 12.7 in DMSO and ACN respectively.[89] This means that at a similar pH, the equilibrium between thiol and thiolate (Scheme 3, *A*) shifts towards

thiol formation. Thus, with a lower amount of thiolate groups, potential for cross-linking decreases.

3.4.2 Hyaluronic acid based hydrogels

Hydrogel formation of HA-MAL and 4arm PEG at various concentrations is listed in Table 7. The lowest concentration for usable hydrogel formation was 0.6% (w/w) HA-MAL and 0.3% (w/w) 4arm PEG. The use of 1X PBS (sample 1[a]) did not yield a hydrogel.

Table 7: Hydrogel formation of HA-MAL and 4arm PEG. [a]Duplicate sample in 1x PBS at pH 4. Percentages are w/w.

Sample	HA-MAL	4arm PEG	Gel	
	Percentage (w/w)	Percentage (w/w)	Directly	After diluting
1[a]	1	0.5	✓[X]	✓[X]
2	0.6	0.3	✓	✓
3	0.5	0.25	✓	✓/X
4	0.4	0.2	✓	X
5	0.3	0.15	X	X
6	0.2	0.1	X	X

An equilibrium shift towards thiol formation instead of thiolate (Scheme 3) is also the case at lower pH. This explains why the duplicate of sample 1 at pH 4 did not form a hydrogel, whereas the same concentration at pH 7 does form a hydrogel. Thus, it is recommended to use HA-MAL and 4arm PEG only at 0.6% and 0.3% (w/w) respectively and at physiological pH.

Hydrogel formation of HA-MAL and 4arm PEG after different preparations is listed in Table 8. Samples 1 and 3 did not yield hydrogels. Hydrogel yielding samples 2 and 4, were somewhat stable when diluting, shown in Figure 22 and Figure 23.

Table 8: Overview HA-MAL hydrogel formation after different preliminary preparations. Percentages are w/w.

| Sample	Properties	Gel	Applied Light Dose for gel formation	Note	Figure
1	1% HA-MAL, 0.5% protected 4arm PEG	X	N/A	Centrifuged, floodlight	Not shown
2	0.6% HA-MAL, 0.15% 4arm PEG, 0.15% protected 4arm PEG	✓	1980 mJ cm^{-2} (3 min)	Centrifuged, 473 nm laser	Figure 22
3	0.6% HA-MAL, 0.12% 4arm PEG, 0.2% protected 4arm PEG	X	N/A	Filtrated through 0.45 µm membrane, 520 nm laser	Not shown
4	0.6% HA-MAL, 0.12% 4arm PEG, 0.2% protected 4arm PEG	✓	2640 mJ cm^{-2} (5 min) to 3696 mJ cm^{-2} (7 min)	520 nm laser	Figure 23
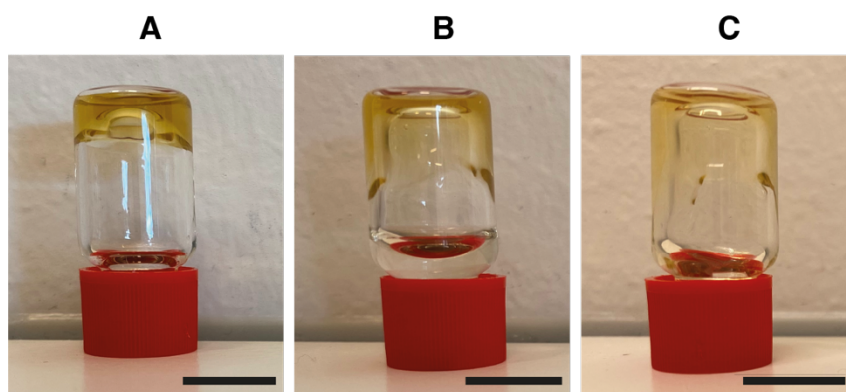
Figure 22: Sample 2 containing a hydrogel of 0.6% HA-MAL, 0.15% 4arm PEG and 0.15% protected 4arm PEG after laser irradiation (λ=473 nm), 3 minutes. A: After printing. B: After addition of 0.5 mL PBS. C: Two days after addition of 0.5 mL PBS. Scale bars represent 10 mm.
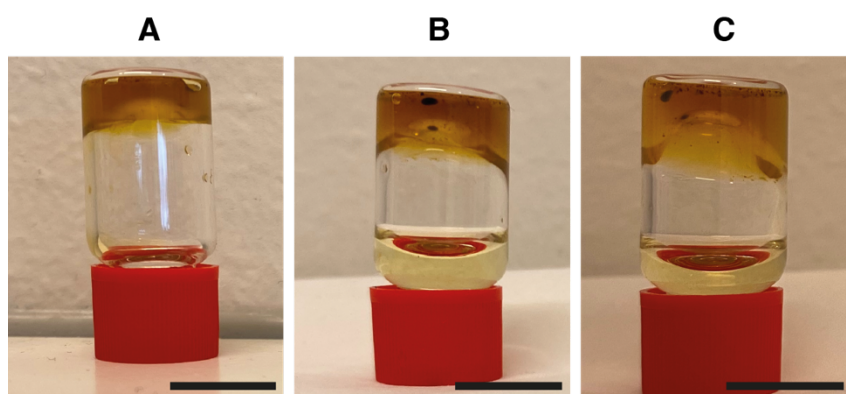

Figure 23: Sample 4 containing a hydrogel of 0.6% HA-MAL hydrogel and 0.3% protected 4arm PEG after laser irradiation (λ=520 nm), 7 minutes. A: After printing. B: After addition of 0.5 mL PBS. C: Five days after addition of 0.5 mL PBS. Scale bars represent 10 mm.

Centrifugation and filtration cannot be used. The latter is a particular problem, since cell printing is done sterilely, and materials are usually filtered through a 0.22 μm filter. The results can be explained when assuming partial dissolution. Undissolved particles are subjected to sedimentation, neither will they pass filters. Also, with increased concentration of *protected 4arm PEG*, the percentage of undissolved particles increases, together with the difference between actual and intended concentrations. For these reasons, samples 1 and 3 (Table 8) made no hydrogel.

Minimizing the loss of *(protected) 4arm PEG* by having a mix of unprotected *4arm PEG* below the hydrogel forming concentration and *protected 4arm PEG* is a method to improve hydrogel formation near λ_{max}, shown by sample 2 (Table 8). It is likely that also at the lower concentration, incomplete dissolution occurred, and some particles were removed by centrifugation, explaining why the hydrogel is weaker than the control and dissolves slowly.

Increasing wavelength to 520 nm was shown to be feasible by sample 4 (Table 8). The lower absorbance is still enough for deprotection, while benefitting from increased light transmittance. It appears that printing time increases when switching from 473 to 520 nm, considering the respective printing times of 3 and 7 minutes, although in the latter case gel formation was already observed after 5 minutes. Although more studies are needed for proper comparisons, longer printing time may be explained by the fact that at increasing wavelength, energy decreases. However, the equipment used for this thesis may explain the

difference also, as the maximum power output of the lasers was different: respectively 1100 and 880 mW for 473 and 520 nm. In case of comparable power output, difference in printing time should decrease.

Protected 4arm PEG having absorbance means that part of the light that travels through the vial is absorbed and the number of photons decreases the further it goes through the material. Depending on the pathlength and intensity of the laser, in case of too high absorbance, it is possible that part of the build construct is irradiated less than intended and printing will not be successful. Bernal *et al.* found a minimum needed light transmittance for LAP of 37% sufficient for printing with 405 nm.[35] Using this parameter to calculate a concentration of *protected 4arm PEG* yields 0.07-0.08 mg/mL. This means that transmittance will be lower than 37% when exceeding this concentration and printability will suffer.

Increasing the light wavelength decreases this problem, as absorbance is lower at wavelengths other than λ_{max} (470 nm). For example, at 520 nm the absorbance is lower therefore the transmittance will be higher. This strategy is widely used with LAP which has a λ_{max} at 375 nm, whereas in VBP 405 nm is used.[35,37–39] An additional benefit of increased wavelength is the reduction of light scattering of precipitating *compound 6* after cleavage, as particles smaller than λ scatter less with increasing wavelength, according to Raleigh Scattering.[90] Particles larger than λ scatter less as well, according to Mie Theory.[91] This is beneficial for printing with cells. The novelty of using 520 nm means that the protected 4arm PEG has potential to be used in multi-material printing.

3.5   Areas for improvement

3.5.1   Increasing uncaging efficiency to reduce printing time

Printing time may also be reduced by increasing uncaging efficiency. A coumarin derivative synthesized by Klimek *et al.*[92] showed 3-4 times increased uncaging compared to *compound 3*, shown in Figure 24 (A). Using a modified version of *compound 6* (B), uncaging should increase. An added benefit when having ethyl as the -R group is a 20 nm bathochromic shift,[92] although it may reduce water solubility.
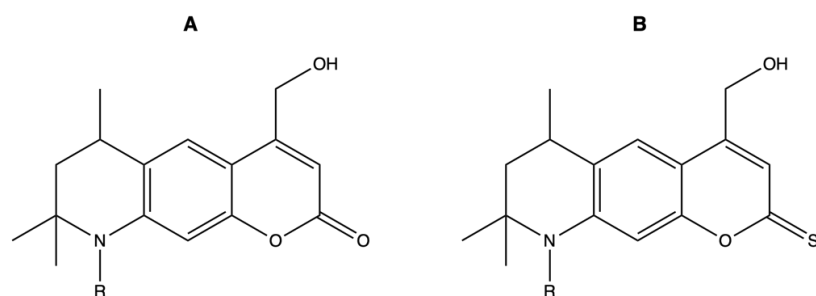
Figure 24: More efficient uncaging coumarin derivative, as synthesized by Klimet et al.[92] B: Potential version of compound 6 with increased uncaging and λ_{max}.

Briefly, the rigidity decreases rotation of the amine, shown in Figure 25. At the excited state (*A*), this amine is normally involved in twisted intramolecular charge transfer (TICT, *B*).[92] Therefore, when photons are absorbed, it leads to (partial) charge transfer from the carbonyl to the amine. Due to this charge interaction with water molecules is increased, releasing energy, and stabilizing the non-excited state. Increased rigidity reduces TICT, increasing decay via the other route of the cleavable bond, and thus uncaging.

Figure 25: Hydrogen bond formation increases decay, adapted from Klimek et al.[92] A: Excitation of coumarin leads to charged carbonyl. In case of compound **6** a similar process happens for the thiocarbonyl. Via the mechanism of intramolecular charge transfer, the amine can becom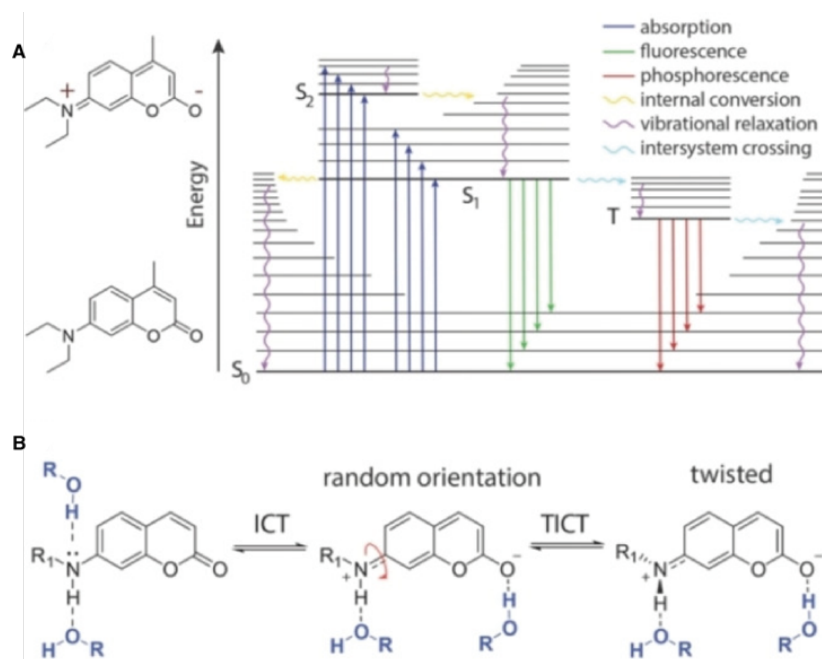e charged as well, shown in B. B: Excitation energy is partially released in the formation of hydrogen bonds between amine and water.

3.5.2   Improving water solubility

Using a longer hydrophilic PEG thiol linker shows promise to negate the low solubility of *compound **6***. Although water solubility of the protected linker may not have been enhanced enough by replacing EDT with 4arm PEG, the difference implies that when using an even longer PEG linker or other more soluble compounds, water solubility will improve further.

A valid consideration is the protection of the hydrogel backbone polymers, as they have good water solubility. Thiol functionalized gelatin and hyaluronic acid are commercially available, which may be protected by PPGs. However, the protection chemistry used for this thesis is incompatible with these, since the reaction is done in DCM, in which they have very low solubility.[93,94] Esterification in water may be possible, but not with the reagents – 4-NPC and DMAP – used in this thesis as they have low water solubility. However, a challenge will be to selectively protect potential thiols on gelatin or hyaluronic acid, since they have amine and alcohol groups that can be conjugated to *compound **6*** in the same reaction.

Another strategy is making *compound **6*** more hydrophilic. Hagen *et al.* showed a more hydrophilic of *compound **3***, shown in Figure 26.[95] Compared to the synthesis scheme of this report, this change cannot be done as a post modification step since it requires a different starting compound. One important consideration is that the substitution of the carbonyl to thiocarbonyl (synthesis of *compound **4** to **5***) needs to be done without the carboxylic acid groups first, since Lawesson's reagent reacts with these.[96] Another challenge will be the higher reactivity of thiocarbonyls in general, increasing the chance of undesirable side reactions.
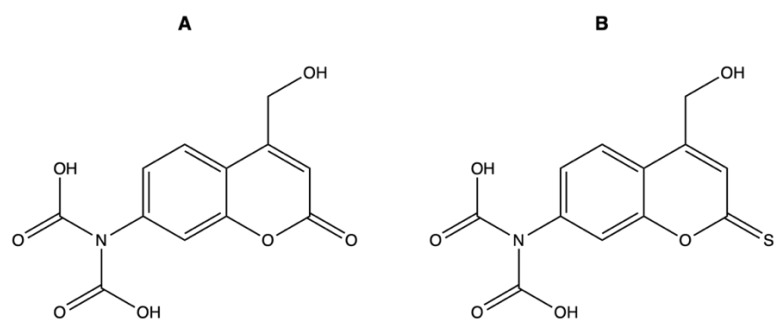
Figure 26: A: More hydrophilic coumarin derivative as synthesized by Hagen et al.[95] The carboxylic acid groups make the molecule more hydrophilic. B: Potential more hydrophilic equivalent to compound 6.

3.5.3   Moving towards physiological ionic strength

Printing of cells using 10X PBS means that their extracellular environment has a far higher salt concentration, shown in Table 9. Thus, cell behavior will change. This is because a significant higher extracellular osmolarity causes cellular water efflux, resulting in shrunken and dehydrated cells.[97]

Table 9: PBS content concentrations.

10X PBS	1X PBS (isotonic to cells)
1.37 M NaCl	0.137 NaCl
0.027 M KCl	0.0027 M KCl
0.119 M Phosphates	0.0119 M Phosphates

Compared to 10X PBS, printing at normal PBS may also be beneficial for thiol-ene reaction kinetics. It was shown that at higher ionic strength, nucleophilic reactions with thiols have longer transition state bonds.[98] Since the transition state theory assumes an equilibrium,[99] the longer the bond, the more the equilibrium moves towards the left.

Reducing hyperosmolarity can be achieved by changing the synthesis of HA-MAL to adjust the pH to pH 6 shortly before freeze-drying. This requires addition of NaOH to the dialyzed solution to form H_2O and NaCl, thus increasing molarity. Since dialysis was done at pH 3.25, using formulas (*3* and *4*), the NaCl increase amounts to $5.6 * 10^{-4}$ M when adjusting to pH 6. Thus, adjusting the pH after dialysis will significantly reduce hyperosmolarity, as normal PBS can be used to bring pH to a physiological level.

$$pH = -\log [H^+]. \tag{3}$$

$$[H^+] = 10^{-pH}. \tag{4}$$

Alternatively, buffer change may also be a strategy to reduce hyperosmolarity. A PBS formulation that is only higher in phosphate concentration, but not in the rest of the salts will have increased buffering capacity while being more isotonic. Considering buffers with a higher buffering capacity to acids is also possible. Good's buffers can be considered, as they are stable, have good water solubility and do not have absorbance or cell toxicity.[100] Examples are tricine and bicine since their respective pKas of 8.05 and 8.26 are higher than the average pKa of 6.8 in PBS.

3.6 Future implications for multi material printing

A start in multi material VBP could be made with using GelMA and the HA-MAL-PEG hydrogel described here. The PI LAP, needed to cross-link GelMA has a λ_{max} of 375 nm, with no absorbance beyond 420 nm. Thus, when mixing both hydrogel solutions together a HA-MAL and protected 4arm PEG hydrogel object could be printed first at 520 nm, with the GelMA printed subsequently at 405 nm.

However, this example demonstrates the need to go beyond free radical cross-linking. Shown in Figure 15 (*C*), HA-MAL degrades into maleic acid that does not react with thiols spontaneously. In presence of free radicals, thiols can become highly reactive thiyl radicals that can react with linear -enes.[101] Shown in Scheme 11 is a potential cross-linking mechanism that ends with transfer of the radical to another thiol. However, also further polymerization to other -enes is possible,[101] leading to non-orthogonal printing.
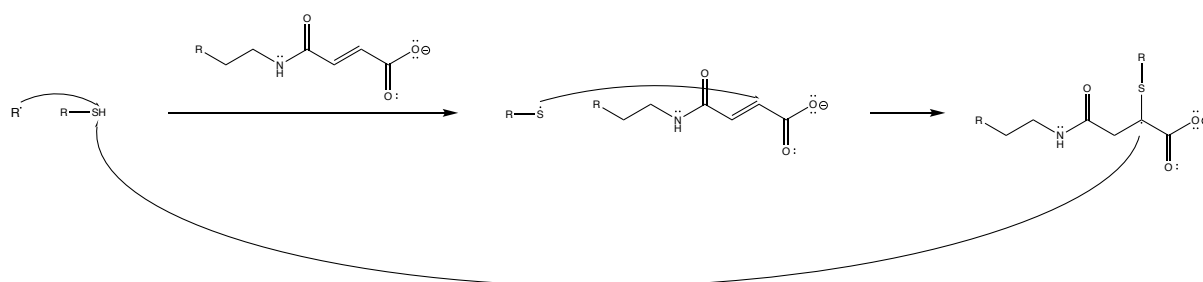
Scheme 11: Potential cross-linking mechanism of thiols to maleic acid. Thiols can form thiyl radicals in presence of free radicals. Their high reactivity may cause them to conjugate to the linear -ene of the maleic acid. After conjugation transfer of the radical to other remaining thiols can occur to repeat the process.

A valid consideration is the possibility of thiols becoming thiyl radicals without free radicals, due to light irradiation. However, thiols have absorbance in the UV region with λ_{max} at 240 nm.[102] Since this wavelength is cytotoxic, it is not to be used in bioprinting. With the use of bioorthogonal wavelengths, thiyl radical formation is unlikely to occur.

A further step towards orthogonal multi material printing could be achieved by using a combination of PPGs that have different absorbance spectra. A requirement will be that only one PPG has absorbance at the selected laser wavelength when printing. In the case of overlap in absorbance spectra at any used wavelength, both protected cross-linkers will become deprotected and undesirable polymerization of both materials will occur.

Such a strategy could include use of HA-MAL and the protection of different thiol linkers with different PPGs. Protective groups could be the green absorbing compound **C** and the violet absorbing compound **E** in Figure 8. A schematic of such a system is shown in Figure 27. In the case of multiple thiol linkers, only one maleimide component can be present. With multiple maleimide components, deprotected thiol linkers will conjugate to multiple maleimide components uncontrollably. However, with surplus of the maleimide component, multi-material printing can be achieved if the thiol linkers themselves are different, due to the formation different hybrid hydrogels. Starting with two protected thiol linkers in presence of excess of maleimide hydrogel molecules, no cross-linking occurs (*A*). When irradiating with one wavelength, one type of thiol linker is deprotected and cross-links, until all has reacted (*B*). Irradiating with the second wavelength deprotect the other thiol linker, the remaining maleimide hydrogel molecules are cross-linked (*C*). Since all components have multiple

reactive groups per molecule, some maleimides may remain free after the first irradiation (*B*), so that some undesired cross-linking may occur after the second irradiation (*C*). To minimize this effect, molar ratios may be adjusted towards favorable kinetics.
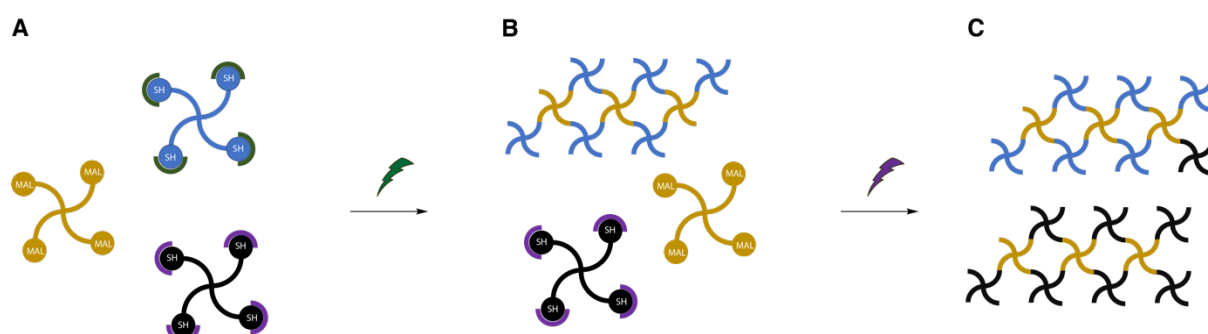

Figure 27: Simplified schematic of thiol-ene multi material printing by the use of maleimide hydrogel molecules and thiol linker protected PPGs. Molar ratios will differ than shown. A: All compounds are unconjugated before light irradiation. B: After green light irradiation, the green absorbing PPG is cleaved after which one thiol linker compound cross-links to HA-MAL. The remaining HA-MAL and the other still protected thiol linker remain in solution. C: After violet light irradiation, the violet absorbing PPG is cleaved after which the other thiol linker cross-links the remaining HA-MAL. When printing with only the maleimide-thiol cross-link system, some of the other thiol linker may cross-link to the earlier formed hydrogel.

In a very recent publication by Rizzo *et al.,*[51] a similar strategy was used using the PPG of Hagen *et al.*[95], Figure 26 (*A*), and taking advantage of the fact that it has selective absorbance for both visible light in single photon irradiation and near infrared light in two-photon irradiation. Sequential printing with both one and two-photon irradiation resulted in a multicellular construct, although one hydrogel type was used. However, in case of uncomplete washing away of unpolymerized materials in between printing steps, or in case of simultaneous multi material printing, non-orthogonal printing may occur as illustrated in Figure 27 (*C*).

Full orthogonality can be achieved by the addition of different cross-linking mechanisms. Li *et al.* reported a light activated bioorthogonal conjugation reaction between phenanthrenequinone (PQ) and vinyl ether (VE), shown in Scheme 12.[103] This mechanism can be used to form hydrogels when first conjugating both components separately to hydrogel backbone molecules. Subsequent combining both materials will produce a hydrogel after light irradiation. When using PQ, fluorescence should be considered as both unconjugated and conjugated PQ have maximum emission at 450 nm.[103] This means if a PPG is chosen that has absorbance around 450 nm, it may be cleaved by local fluorescence of PQ, even if the light sources used are outside of the PPG's absorbance spectrum.
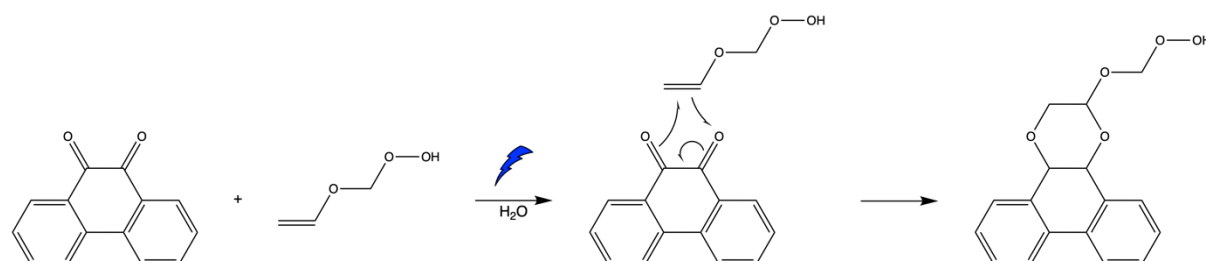
Scheme 12: Conjugation mechanism of phenanthrenequinone to vinyl ether.

An example of true multi material printing is illustrated in Figure 28. When dissolving HA-MAL, protected 4arm PEG, PQ functionalized gelatin, and VE functionalized gelatin, all compounds will be free in solution before light irradiation (*A*). After green light irradiation, deprotection

of protected 4arm PEG will occur and a HA-MAP-PEG hydrogel will form due to thiol-maleimide cross-linking (*B*). The PQ- and VE functionalized gelatin will remain in solution, until irradiation with blue light, after which these form a gelatin hydrogel (*C*). Due to two incompatible conjugation chemistries, full orthogonality is achieved.
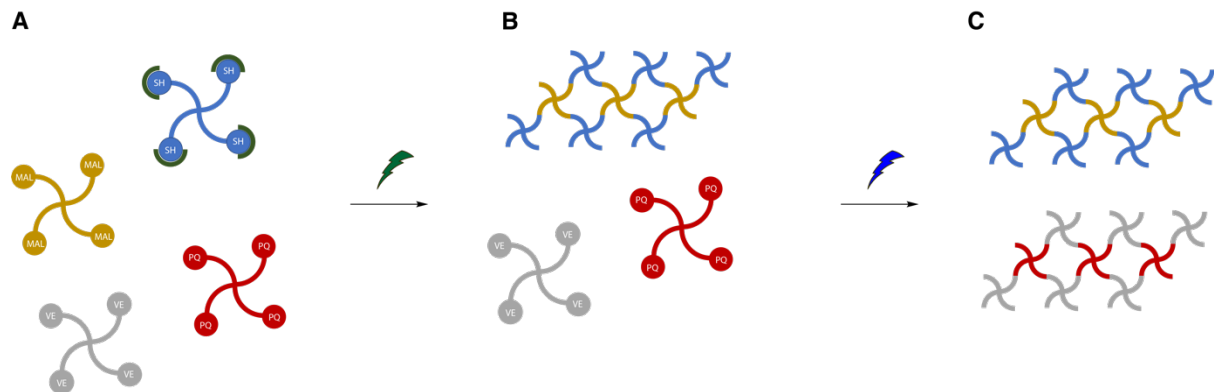

Figure 28: Orthogonal multi material printing by combining a thiol-maleimide and a PQ-VE hydrogel. A: All compounds are unconjugated before light irradiation. B: After green light irradiation, deprotection of thiols results in thiol-maleimide cross-links and hydrogel formation. C: After blue light irradiation, PQ and VE cross-link, forming another hydrogel.

4   Conclusion

In this thesis, it was shown that synthesis of a green absorbing PPG to protect thiolated PEG is an attainable approach. Also, HA-MAL can be functionalized to a degree that cross-linking occurs rapidly and that a strong enough hydrogel is produced. The HA-MAL synthesized in this thesis produced a strong hydrogel at only 3% (w/w) that lasted several weeks when diluting with PBS. This property makes it an attractive material for bioprinting. It was demonstrated that use of these materials in a novel bio-ink is feasible, as hydrogels were produced by novel use of laser wavelengths 473 and 520 nm. This achievement forms an attractive prospect for multi material printing. Short term multi material printing may be explored by combining GelMA with HA-MAL or combining HA-MAL with different protected thiol linkers, although they are likely not entirely orthogonal. Future true multi material VBP may be achieved by combining multiple orthogonal conjugation chemistries of which thiol-maleimide chemistry is likely to be part of. Although further refinements of the solubility of the PPG and pH neutralization of HA-MAL solutions that were used here are needed, this thesis demonstrates that HA-MAL and PPG protected thiolated compounds have great promise to become essential materials for bio-inks in bioorthogonal multi material VBP.

References

1. Vanholder, R. *et al.* Organ donation and transplantation: a multi-stakeholder call to action. *Nat. Rev. Nephrol.* **17**, 554–568 (2021).
2. Lewis, A. *et al.* Organ donation in the US and Europe: The supply vs demand imbalance. *Transplant. Rev.* **35**, 100585 (2021).
3. Committee on Issues in Organ Donor Intervention Research, Board on Health Sciences Policy, Health and Medicine Division, & National Academies of Sciences, Engineering, and Medicine. *Opportunities for Organ Donor Intervention Research: Saving Lives by Improving the Quality and Quantity of Organs for Transplantation.* 24884 (National Academies Press, 2017). doi:10.17226/24884.
4. Hasan, A. *Tissue engineering for artificial organs: regenerative medicine, smart diagnostics and personalized medicine.* (Wiley-VCH, 2017).
5. Groll, J. *et al.* Biofabrication: reappraising the definition of an evolving field. *Biofabrication* **8**, 013001 (2016).
6. Guillemot, F., Mironov, V. & Nakamura, M. Bioprinting is coming of age: report from the International Conference on Bioprinting and Biofabrication in Bordeaux (3B'09). *Biofabrication* **2**, 010201 (2010).
7. Malda, J. *et al.* 25th Anniversary Article: Engineering Hydrogels for Biofabrication. *Adv. Mater.* **25**, 5011–5028 (2013).
8. Koch, L., Gruene, M., Unger, C. & Chichkov, B. Laser Assisted Cell Printing. *Curr. Pharm. Biotechnol.* **14**, 91–97 (2013).
9. Derby, B. Bioprinting: inkjet printing proteins and hybrid cell-containing materials and structures. *J. Mater. Chem.* **18**, 5717 (2008).
10. Nakamura, M. *et al.* Biocompatible Inkjet Printing Technique for Designed Seeding of Individual Living Cells. *Tissue Eng.* **11**, 1658–1666 (2005).
11. Duarte Campos, D. F. *et al.* Three-dimensional printing of stem cell-laden hydrogels submerged in a hydrophobic high-density fluid. *Biofabrication* **5**, 015003 (2012).
12. Naghieh, S. & Chen, X. Printability–A key issue in extrusion-based bioprinting. *J. Pharm. Anal.* **11**, 564–579 (2021).
13. Ribeiro, A. *et al.* Assessing bioink shape fidelity to aid material development in 3D bioprinting. *Biofabrication* **10**, 014102 (2017).
14. Park, S., Jung, W.-H., Pittman, M., Chen, J. & Chen, Y. The Effects of Stiffness, Fluid Viscosity, and Geometry of Microenvironment in Homeostasis, Aging, and Diseases: A Brief Review. *J. Biomech. Eng.* **142**, 100804 (2020).
15. Schwab, A. *et al.* Printability and Shape Fidelity of Bioinks in 3D Bioprinting. *Chem. Rev.* **120**, 11028–11055 (2020).
16. Razzak, M. T., Darwis, D., Zainuddin, & Sukirno. Irradiation of polyvinyl alcohol and polyvinyl pyrrolidone blended hydrogel for wound dressing. *Radiat. Phys. Chem.* **62**, 107–113 (2001).
17. Ma, Q., Moldovan, N., Mancini, D. C. & Rosenberg, R. A. Synchrotron-radiation-induced, selective-area deposition of gold on polyimide from solution. *Appl. Phys. Lett.* **76**, 2014–2016 (2000).
18. Pathak, C. P., Sawhney, A. S. & Hubbell, J. A. Rapid photopolymerization of immunoprotective gels in contact with cells and tissue. *J. Am. Chem. Soc.* **114**, 8311–8312 (1992).
19. Wei, H.-L., Yang, Z., Zheng, L.-M. & Shen, Y.-M. Thermosensitive hydrogels synthesized by fast Diels–Alder reaction in water. *Polymer* **50**, 2836–2840 (2009).
20. Rokita, B., Rosiak, J. M. & Ulanski, P. Ultrasound-Induced Cross-Linking and Formation of Macroscopic Covalent Hydrogels in Aqueous Polymer and Monomer Solutions. *Macromolecules* **42**, 3269–3274 (2009).
21. Peppas, N. A., Moynihan, H. J. & Lucht, L. M. The structure of highly crosslinked poly(2-hydroxyethyl methacrylate) hydrogels. *J. Biomed. Mater. Res.* **19**, 397–411 (1985).
22. Hirst, A. R., Escuder, B., Miravet, J. F. & Smith, D. K. High-Tech Applications of Self-Assembling Supramolecular Nanostructured Gel-Phase Materials: From Regenerative Medicine to Electronic Devices. *Angew. Chem. Int. Ed.* **47**, 8002–8018 (2008).
23. Wang, P., Deng, G., Zhou, L., Li, Z. & Chen, Y. Ultrastretchable, Self-Healable Hydrogels Based on Dynamic Covalent Bonding and Triblock Copolymer Micellization. *ACS Macro Lett.* **6**, 881–886 (2017).
24. Kumar, H. & Kim, K. Stereolithography 3D Bioprinting. in *3D Bioprinting: Principles and Protocols* (ed. Crook, J. M.) 93–108 (Springer US, 2020). doi:10.1007/978-1-0716-0520-2_6.
25. Zhu, W. *et al.* Direct 3D bioprinting of prevascularized tissue constructs with complex microarchitecture. *Biomaterials* **124**, 106–115 (2017).
26. Khalil, S. & Sun, W. Bioprinting Endothelial Cells With Alginate for 3D Tissue Constructs. *J. Biomech. Eng.* **131**, 111002 (2009).
27. Ballermann, B. J., Dardik, A., Eng, E. & Liu, A. Shear stress and the endothelium. *Kidney Int.* **54**, S100–S108 (1998).
28. Ren, Y. *et al.* Developments and Opportunities for 3D Bioprinted Organoids. *Int. J. Bioprinting* **7**, 364 (2021).
29. Mau, R., Nazir, J., John, S. & Seitz, H. Preliminary Study on 3D printing of PEGDA Hydrogels for Frontal Sinus Implants using Digital Light Processing (DLP). *Curr. Dir. Biomed. Eng.* **5**, 249–252 (2019).
30. Jakab, K., Damon, B., Neagu, A., Kachurin, A. & Forgacs, G. Three-dimensional tissue constructs built by bioprinting. *Biorheology* **43**, 509–513 (2006).
31. Brunel, L. G., Hull, S. M. & Heilshorn, S. C. Engineered assistive materials for 3D bioprinting: support baths and sacrificial inks. *Biofabrication* **14**, 032001 (2022).
32. Muthusamy, M., Safaee, S. & Chen, R. Additive Manufacturing of Overhang Structures Using Moisture-Cured Silicone with Support Material. *J. Manuf. Mater. Process.* **2**, 24 (2018).
33. Abdel Fattah, A. R. *et al.* In Situ 3D Label-Free Contactless Bioprinting of Cells through Diamagnetophoresis. *ACS Biomater. Sci. Eng.* **2**, 2133–2138 (2016).
34. Marx, V. Biophysics: using sound to move cells. *Nat. Methods* **12**, 41–44 (2015).
35. Bernal, P. N. *et al.* Volumetric Bioprinting of Complex Living-Tissue Constructs within Seconds. *Adv. Mater.* **31**, 1904209 (2019).
36. Kak, A. C., Slaney, M. & Wang, G. Principles of Computerized Tomographic Imaging. *Med. Phys.* **29**, 107–107 (2002).
37. Bernal, P. N. *et al.* Volumetric Bioprinting of Organoids and Optically Tuned Hydrogels to Build Liver-Like Metabolic Biofactories. *Adv. Mater.* **34**, 2110054 (2022).
38. Gehlen, J., Qiu, W., Schädli, G. N., Müller, R. & Qin, X.-H. Tomographic volumetric bioprinting of heterocellular bone-like tissues in seconds. *Acta Biomater.* **156**, 49–60 (2023).
39. Rizzo, R., Ruetsche, D., Liu, H. & Zenobi-Wong, M. Optimized Photoclick (Bio)Resins for Fast Volumetric Bioprinting. *Adv. Mater.* **33**, 2102900 (2021).
40. Lee, M., Rizzo, R., Surman, F. & Zenobi-Wong, M. Guiding Lights: Tissue Bioprinting Using Photoactivated Materials. *Chem. Rev.* **120**, 10950–11027 (2020).

41. Benton, J. A., DeForest, C. A., Vivekanandan, V. & Anseth, K. S. Photocrosslinking of Gelatin Macromers to Synthesize Porous Hydrogels That Promote Valvular Interstitial Cell Function. *Tissue Eng. Part A* **15**, 3221–3230 (2009).

42. Michon, C., Cuvelier, G. & Launay, B. Concentration dependence of the critical viscoelastic properties of gelatin at the gel point. *Rheol. Acta* **32**, 94–103 (1993).

43. Van Den Bulcke, A. I. *et al.* Structural and Rheological Properties of Methacrylamide Modified Gelatin Hydrogels. *Biomacromolecules* **1**, 31–38 (2000).

44. Pepelanova, I., Kruppa, K., Scheper, T. & Lavrentieva, A. Gelatin-Methacryloyl (GelMA) Hydrogels with Defined Degree of Functionalization as a Versatile Toolkit for 3D Cell Culture and Extrusion Bioprinting. *Bioengineering* **5**, 55 (2018).

45. Xu, X., Jha, A. K., Harrington, D. A., Farach-Carson, M. C. & Jia, X. Hyaluronic Acid-Based Hydrogels: from a Natural Polysaccharide to Complex Networks. *Soft Matter* **8**, 3280–3294 (2012).

46. Fraser, J. R. E., Laurent, T. C. & Laurent, U. B. G. Hyaluronan: its nature, distribution, functions and turnover. *J. Intern. Med.* **242**, 27–33 (1997).

47. Smeds, K. A., Pfister-Serres, A., Hatchell, D. L. & Grinstaff, M. W. Synthesis of a Novel Polysaccharide Hydrogel. *J. Macromol. Sci. Part A* **36**, 981–989 (1999).

48. Smeds, K. A. & Grinstaff, M. W. Photocrosslinkable polysaccharides forin situ hydrogel formation. *J. Biomed. Mater. Res.* **54**, 115–121 (2001).

49. Melchels, F. P. W., Dhert, W. J. A., Hutmacher, D. W. & Malda, J. Development and characterisation of a new bioink for additive tissue manufacturing. *J. Mater. Chem. B* **2**, 2282 (2014).

50. Xavier, J. R. *et al.* Bioactive Nanoengineered Hydrogels for Bone Tissue Engineering: A Growth-Factor-Free Approach. *ACS Nano* **9**, 3109–3118 (2015).

51. Rizzo, R., Petelinšek, N., Bonato, A. & Zenobi-Wong, M. From Free-Radical to Radical-Free: A Paradigm Shift in Light-Mediated Biofabrication. *Adv. Sci.* 2205302 (2023) doi:10.1002/advs.202205302.

52. Sun, M. *et al.* Synthesis and Properties of Gelatin Methacryloyl (GelMA) Hydrogels and Their Recent Applications in Load-Bearing Tissue. *Polymers* **10**, 1290 (2018).

53. Simon, H.-U., Haj-Yehia, A. & Levi-Schaffer, F. Role of reactive oxygen species (ROS) in apoptosis induction. *Apoptosis* **5**, 415–418 (2000).

54. Valencia, A. & Morán, J. Reactive oxygen species induce different cell death mechanisms in cultured neurons. *Free Radic. Biol. Med.* **36**, 1112–1125 (2004).

55. Vroegop, S. Localization of damage induced by reactive oxygen species in cultured cells. *Free Radic. Biol. Med.* **18**, 141–151 (1995).

56. Freeman, B. A. & Crapo, J. D. Biology of disease: free radicals and tissue injury. *Lab. Investig. J. Tech. Methods Pathol.* **47**, 412–426 (1982).

57. Fiers, W., Beyaert, R., Declercq, W. & Vandenabeele, P. More than one way to die: apoptosis, necrosis and reactive oxygen damage. *Oncogene* **18**, 7719–7730 (1999).

58. Davalli, P., Marverti, G., Lauriola, A. & D'Arca, D. Targeting Oxidatively Induced DNA Damage Response in Cancer: Opportunities for Novel Cancer Therapies. *Oxid. Med. Cell. Longev.* **2018**, 2389523 (2018).

59. Clayden, J., Greeves, N. & Warren, S. G. *Organic chemistry*. (Oxford University Press, 2012).

60. Klán, P. *et al.* Photoremovable Protecting Groups in Chemistry and Biology: Reaction Mechanisms and Efficacy. *Chem. Rev.* **113**, 119–191 (2013).

61. Hansen, M. J., Velema, W. A., Lerch, M. M., Szymanski, W. & Feringa, B. L. Wavelength-selective cleavage of photoprotecting groups: strategies and applications in dynamic systems. *Chem. Soc. Rev.* **44**, 3358–3377 (2015).

62. Yang, H., Zhang, X., Zhou, L. & Wang, P. Development of a Photolabile Carbonyl-Protecting Group Toolbox. *J. Org. Chem.* **76**, 2040–2048 (2011).

63. Aujard, I. *et al.* o-Nitrobenzyl Photolabile Protecting Groups with Red-Shifted Absorption: Syntheses and Uncaging Cross-Sections for One- and Two-Photon Excitation. *Chem. - Eur. J.* **12**, 6865–6879 (2006).

64. Er-Rhaimini, A., Mohsinaly, N. & Mornet, R. The photosolvolysis of N-arylmethyladenines. Photoremovable N-arylmethyl protective groups for N-containing compounds. *Tetrahedron Lett.* **31**, 5757–5760 (1990).

65. Fournier, L. *et al.* A Blue-Absorbing Photolabile Protecting Group for *in Vivo* Chromatically Orthogonal Photoactivation. *ACS Chem. Biol.* **8**, 1528–1536 (2013).

66. Kotzur, N., Briand, B., Beyermann, M. & Hagen, V. Wavelength-Selective Photoactivatable Protecting Groups for Thiols. *J. Am. Chem. Soc.* **131**, 16927–16931 (2009).

67. Goguen, B. N., Aemissegger, A. & Imperiali, B. Sequential Activation and Deactivation of Protein Function Using Spectrally Differentiated Caged Phosphoamino Acids. *J. Am. Chem. Soc.* **133**, 11038–11041 (2011).

68. Rodrigues-Correia, A., Weyel, X. M. M. & Heckel, A. Four Levels of Wavelength-Selective Uncaging for Oligonucleotides. *Org. Lett.* **15**, 5500–5503 (2013).

69. Menge, C. & Heckel, A. Coumarin-Caged dG for Improved Wavelength-Selective Uncaging of DNA. *Org. Lett.* **13**, 4620–4623 (2011).

70. Velema, W. A., van der Berg, J. P., Szymanski, W., Driessen, A. J. M. & Feringa, B. L. Orthogonal Control of Antibacterial Activity with Light. *ACS Chem. Biol.* **9**, 1969–1974 (2014).

71. Priestman, M. A., Sun, L. & Lawrence, D. S. Dual Wavelength Photoactivation of cAMP- and cGMP-Dependent Protein Kinase Signaling Pathways. *ACS Chem. Biol.* **6**, 377–384 (2011).

72. Olson, J. P. *et al.* Optically Selective Two-Photon Uncaging of Glutamate at 900 nm. *J. Am. Chem. Soc.* **135**, 5954–5957 (2013).

73. Nguyen, L.-T. T., Gokmen, M. T. & Du Prez, F. E. Kinetic comparison of 13 homogeneous thiol–X reactions. *Polym. Chem.* **4**, 5527 (2013).

74. Sun, Y. *et al.* Thiol Michael addition reaction: a facile tool for introducing peptides into polymer-based gene delivery systems: Thiol Michael addition reaction for introducing peptides. *Polym. Int.* **67**, 25–31 (2018).

75. Kakwere, H. & Perrier, S. Orthogonal "Relay" Reactions for Designing Functionalized Soft Nanoparticles. *J. Am. Chem. Soc.* **131**, 1889–1895 (2009).

76. Lowe, A. B. Thiol-ene "click" reactions and recent applications in polymer and materials synthesis. *Polym Chem* **1**, 17–36 (2010).

77. Gennari, A., Wedgwood, J., Lallana, E., Francini, N. & Tirelli, N. Thiol-based michael-type addition. A systematic evaluation of its controlling factors. *Tetrahedron* **76**, 131637 (2020).

78. Klimek, R. *et al.* Visible light-activatable Q-dye molecular beacons for long-term mRNA monitoring in neurons. *Chem. Commun.* **57**, 12683–12686 (2021).

79. Weinrich, T., Gränz, M., Grünewald, C., Prisner, T. F. & Göbel, M. W. Synthesis of a Cytidine Phosphoramidite with Protected Nitroxide Spin Label for EPR Experiments with RNA. *Eur. J. Org. Chem.* **2017**, 491–496 (2017).
80. Liao, F. *et al.* Facile one-step coating approach to magnetic submicron particles with poly(ethylene glycol) coats and abundant accessible carboxyl groups. *Int. J. Nanomedicine* 791 (2013) doi:10.2147/IJN.S41411.
81. Gilles, M. A., Hudson, A. Q. & Borders, C. L. Stability of water-soluble carbodiimides in aqueous solution. *Anal. Biochem.* **184**, 244–248 (1990).
82. Hussein, E. M. A. *Radiation Mechanics*. (Elsevier, 2007). doi:10.1016/B978-0-08-045053-7.X5000-9.
83. Chen, D., Yang, C. Q. & Qiu, X. Aqueous Polymerization of Maleic Acid and Cross-Linking of Cotton Cellulose by Poly(maleic acid). *Ind. Eng. Chem. Res.* **44**, 7921–7927 (2005).
84. Northrop, B. H., Frayne, S. H. & Choudhary, U. Thiol–maleimide "click" chemistry: evaluating the influence of solvent, initiator, and thiol on the reaction mechanism, kinetics, and selectivity. *Polym. Chem.* **6**, 3415–3430 (2015).
85. Kharkar, P. M., Kloxin, A. M. & Kiick, K. L. Dually degradable click hydrogels for controlled degradation and protein release. *J Mater Chem B* **2**, 5511–5521 (2014).
86. Lust, S. T. *et al.* Selectively Cross-Linked Tetra-PEG Hydrogels Provide Control over Mechanical Strength with Minimal Impact on Diffusivity. *ACS Biomater. Sci. Eng.* **7**, 4293–4304 (2021).
87. Tan, H., DeFail, A. J., Rubin, J. P., Chu, C. R. & Marra, K. G. Novel multiarm PEG-based hydrogels for tissue engineering. *J. Biomed. Mater. Res. A* **9999A**, NA-NA (2009).
88. Galindo, F. The photochemical rearrangement of aromatic ethers. *J. Photochem. Photobiol. C Photochem. Rev.* **6**, 123–138 (2005).
89. Rossini, E. On the computation of pKa values of organic and organometallic molecules in different solvents. 148 Seiten (2017) doi:10.17169/REFUBIUM-9995.
90. Rayleigh, Lord. XLII. *On the scattering of light by a cloud of similar small particles of any shape and oriented at random*. *Lond. Edinb. Dublin Philos. Mag. J. Sci.* **35**, 373–381 (1918).
91. Mie, G. Beiträge zur Optik trüber Medien, speziell kolloidaler Metallösungen. *Ann. Phys.* **330**, 377–445 (1908).
92. Klimek, R. *et al.* Inactivation of Competitive Decay Channels Leads to Enhanced Coumarin Photochemistry. *Chem. – Eur. J.* **28**, (2022).
93. Jeanloz, R. W. & Forchielli, E. Studies on hyaluronic acid and related substances. I. Preparation of hyaluronic acid and derivatives from human umbilical cord. *J. Biol. Chem.* **186**, 495–511 (1950).
94. Ward, A. G. & Courts, A. *The science and technology of gelatin*. (Academic Press, 1977).
95. Hagen, V. *et al.* Coumarinylmethyl Esters for Ultrafast Release of High Concentrations of Cyclic Nucleotides upon One- and Two-Photon Photolysis. *Angew. Chem. Int. Ed.* **44**, 7887–7891 (2005).
96. Rao, Y., Li, X., Nagorny, P., Hayashida, J. & Danishefsky, S. J. A simple method for the conversion of carboxylic acids into thioacids with Lawesson's reagent. *Tetrahedron Lett.* **50**, 6684–6686 (2009).
97. Reinehr, R. & Haussinger, D. Hyperosmotic activation of the CD95 death receptor system. *Acta Physiol.* **187**, 199–203 (2006).
98. Pham, T. V. & Westaway, K. C. Solvent effects on nucleophilic substitution reactions. III. The effect of adding an inert salt on the structure of the S_N2 transition state. *Can. J. Chem.* **74**, 2528–2530 (1996).
99. *The IUPAC Compendium of Chemical Terminology: The Gold Book*. (International Union of Pure and Applied Chemistry (IUPAC), 2019). doi:10.1351/goldbook.
100. Good, N. E. *et al.* Hydrogen Ion Buffers for Biological Research. *Biochemistry* **5**, 467–477 (1966).
101. Coote, M. L. & Degirmenci, I. Theory and Applications of Thiyl Radicals in Polymer Chemistry. in *Computational Quantum Chemistry* 195–218 (Elsevier, 2019). doi:10.1016/B978-0-12-815983-5.00006-4.
102. Polgár, L. Spectrophotometric determination of mercaptide ion, an activated form of SH-group in thiol enzymes. *FEBS Lett.* **38**, 187–190 (1974).
103. Li, J. *et al.* Visible Light-Initiated Bioorthogonal Photoclick Cycloaddition. *J. Am. Chem. Soc.* **140**, 14542–14546 (2018).